1 **Title:** *Corylus avellana* disease management: using metagenomics to illuminate the rhizosphere

2 microbiome of hazelnut

3

4 **Authors:** John K. Robinson[1], John M. Steele[1], Thomas J. Molnar[2], Sharon Regan[1], George C.

5 diCenzo[1*]

6

7 **Affiliations:** [1] Department of Biology, Queen's University, Kingston, Ontario, Canada

8 [2] Department of Plant Biology, Rutgers University, Newark, New Jersey, USA

9

10 *** Corresponding author:** George C. diCenzo, george.dicenzo@queensu.ca

11

12 **Keywords:** Hazelnut, Rhizosphere, Metagenomics, Microbiome, Plant-Microbe Interaction

ABSTRACT

The European hazelnut, *Corylus avellana*, is one of the most economically important tree nut crops globally. The biotrophic ascomycete pathogen *Anisogramma anomala*, found naturally associated with wild *C. americana*, continues to pose a significant threat to European hazelnut production across North America. Here, metagenomics was used to examine the taxonomic and functional features of the rhizosphere microbial communities of hazelnut trees differing in their levels of resistance to *A. anomala*: highly tolerant *Corylus americana*, and resistant and susceptible *Corylus avellana*. No statistically significant differences in microbial alpha diversity or beta diversity were noted between the three rhizosphere groups. Compared to bulk soil, all three rhizosphere groups were enriched for the fungal phylum Basidiomycota and bacterial phylum "*Candidatus* Rokubacteriota". At the genus level, the bacterial genera *Actinospica*, *Occallatibacter*, and "*Candidatus* Sulfotelmatobacter" were under-represented, while the genus *Rhizobacter* was over-represented, in the resistant and susceptible *C. avellana* rhizosphere samples compared to the bulk soil. A total of 45 dereplicated, high-quality metagenome-assembled genomes (MAGs) were generated, corresponding to 41 bacteria and 4 archaea. Many of the MAGs carried multiple biosynthetic gene clusters, including MAGs corresponding to the genera *Lysobacter* and *Actinospica*. Overall, the low differentiation of the rhizosphere microbiomes suggest that differences in *A. anomala* disease expression are likely not associated with differences in the rhizosphere microbiome. Nevertheless, the results shed new light on the rhizosphere communities of two species of hazelnut, and woody perennials more broadly, and identify potential avenues for future research into the development of microbial inoculants for *Corylus* spp..

34 **INTRODUCTION**

35 Hazelnut cultivation has a rich history and is still of economic importance in contemporary
36 societies. The European hazelnut *Corylus avellana* has been cultivated since Roman times
37 (Boccacci and Botta 2009) and remains one of the world's principal tree nut crops (Helmstetter et
38 al. 2020). Approximately 70% percent of the world's hazelnuts are presently grown in Turkey
39 (Food and Agricultural Organization of the United Nations 2021), but the future of Turkey's
40 hazelnut industry remains uncertain. To stabilize existing hazelnut production and supply growing
41 global demand, the world's hazelnut orchards must expand across suitable growing regions.
42 Historically, commercial production of *C. avellana* in North America outside of the Pacific
43 Northwest was limited due to the devastating impact of the biotrophic ascomycete pathogen
44 *Anisogramma anomala* (Molnar 2011; Revord et al. 2020; Thompson et al. 1996). Unlike the
45 native but not-commercially amenable American hazelnut species, *Corylus americana*, that is
46 native to North America and resistant or highly tolerant of *A. anomala* infection, European
47 hazelnut is generally highly susceptible. In susceptible hosts, *A. anomala* infection results in the
48 formation of perennial cankers that girdle branches, culminating in tree death (Pinkerton 1995).
49 Current management practices are both costly and labour intensive relying on pruning and large
50 quantities of fungicides (Jeger et al. 2018). Further, it is documented that the *C. avellana* host
51 protection imparted through widely disseminated resistance (R) genes from *C. avellana* 'Gasaway'
52 in Oregon and other R genes mapped to the same linkage group, have been overcome in certain
53 regions (Jacobs et al. 2024a). Consequently, there is a pressing need to identify alternate strategies,
54 such as biocontrol, to reduce the impact of *A. anomala* on hazelnut cultivation.

55 A potential source of biocontrol agents is the native microbial community associated with
56 a plant species of interest. The plant microbiome is typically divided into three major regions: the

57 phyllosphere, representing the above-ground surface regions occupied by microbes; the
58 endosphere, representing the regions comprised of the plant's inner tissues; and the rhizosphere,
59 which refers to the thin layer of soil surrounding plant roots (Gupta et al. 2021; Santoyo 2022;
60 Zhang et al. 2021). The rhizosphere ecosystem is particularly complex (Jones and Hinsinger 2008)
61 laden with an exceptional diversity of life (Dlamini et al. 2022; Zhang et al. 2020). These plant
62 root-associated microbial communities have been referred to as the plant's second genome
63 (Berendsen et al. 2012), as they are capable of profoundly extending the plant's functional
64 potential (Bakker et al. 2013a). Notable examples of plant benefits conferred through these
65 associations include enhanced nutrient availability and improved tolerance to both biotic and
66 abiotic stress (Bakker et al. 2013b; Hakim et al. 2021; Pantigoso et al. 2022).

67 Importantly, rhizosphere microbial populations can be influenced by both the plant
68 genotype and its disease state (Liu et al. 2019; Liu et al. 2021; Liu et al. 2023a). Though conflicting
69 evidence has been reported (Fitzpatrick et al. 2018), increasing host plant phylogenetic distance
70 has been associated with less similar bacterial rhizosphere composition (Bouffaud et al. 2014; Lei
71 et al. 2019; Liu et al. 2023b), while two genotypes of the same plant species can possess similar
72 but distinguishable microbial populations (Peiffer et al. 2013). Likewise, domestication has been
73 found to influence microbiome assembly and metabolic functions (Yue et al. 2023).

74 At the same time, rhizosphere microbial communities may be modified based on plant root
75 secretions, with plants potentially recruiting and stimulating disease suppressive microbial taxa in
76 response to pathogens as a means of improving disease outcomes (Liu et al. 2023a). Rhizosphere
77 microbes may mitigate plant disease through antagonistic microbe-microbe interactions (Hassani
78 et al. 2018), priming of the plant immune system via induced systemic resistance (ISR) (Yu et al.
79 2022), and enhanced nutrient acquisition (Dordas 2008; Dotaniya and Meena 2015). Microbes that

80 exhibit these properties may therefore prove useful in disease management, through serving as
81 biopesticides, enhancing systemic plant disease tolerance through eliciting ISR, or by bolstering
82 overall plant vigour through facilitating nutrient acquisition. The rhizosphere microbiome is
83 therefore worth examining as a promising reservoir of disease attenuating agents, and
84 characterizing interactions between plant roots and their surrounding organisms has demonstrated
85 extensive promise for the improvement of economically valuable crops (Orozco-Mosqueda et al.
86 2022).

87 Unfortunately, the rhizosphere of woody perennial plants remains understudied relative to
88 annual crops. Despite the relative paucity of research in this area, the diverse utility of woody
89 perennial associated rhizosphere microbes has been validated by numerous studies. For example,
90 phosphate solubilizing microbes with plant growth promoting potential have been reported in the
91 peach rhizosphere (Li et al. 2025), highlighting the prospect of leveraging rhizosphere microbial
92 communities to enhance woody perennial vigour. In addition, the promise of certain walnut-
93 associated plant growth-promoting rhizobacteria (PGPR) for enhancing drought tolerance (Lotfi
94 et al. 2022) illustrates the abiotic stress ameliorating potential of microbes in the woody perennial
95 rhizosphere. Further, examples of the capacity of rhizosphere microbes to aid in combating biotic
96 stress have been reported for woody perennial crops including apple (Berdeni et al. 2018;
97 Derikvand et al. 2023), pear (Zhang et al. 2023), plum (Ali et al. 2018), and citrus (Ezrari et al.
98 2021). Collectively, these studies suggest woody perennial rhizosphere microbes may aid in
99 addressing several significant challenges facing woody perennial cultivation.

100 In the current study, shotgun metagenomics was used to investigate the rhizosphere
101 microbiome of North American grown hazelnut plants. To investigate the effect of genotype and
102 disease resistant phenotypes, samples were collected from an orchard infected with *A. anomala*

103 and were taken from the rhizospheres of native *C. americana* plants and *C. avellana* genotypes
104 that are resistant or susceptible to *A. anomala* infection. By gaining insight into the taxonomic and
105 functional features of hazelnut trees, this study broadens the scope of available genomic
106 information relevant to hazelnut improvement, including for disease management, and may help
107 guide future identification of biocontrol agents.
108

109 METHODS

110 Soil sample collection

111 Bulk soil and rhizosphere samples were collected from Hort Farm 3, 67 Ryders Lane, East
112 Brunswick, NJ 08816, between 1:00 PM and 4:00 PM on 19 October 2022. Soils were collected
113 using a small shovel that was sterilized with 70% ethanol before each sample collection, and
114 transferred to sterile 50 mL tubes. Soils from highly tolerant *C. americana* trees were collected
115 from row 1 of the farm. Soils from *C. avellana* trees collected from row 3 were divided into two
116 groups segregating for disease resistance, designated resistant and susceptible, based on the
117 presence or absence of pronounced *A. anomala* cankers. Five soil samples were collected for each
118 of the three hazelnut varieties; samples were collected at a depth of approximately 15 cm,
119 approximately 15 cm away from the trunk of the tree. In addition, five bulk soil samples were
120 collected at a depth of approximately 15 cm from five sites around the periphery of the hazelnut
121 orchard.
122

123 DNA isolation and sequencing

124 Approximately one hour after sample collection was complete, ~0.42 g subsamples of soil were
125 taken from each soil sample. DNA extraction was performed using a Qiagen DNeasy PowerSoil

126 Pro Kit, according to the manufacturer's instructions. One of the bulk soil samples was omitted
127 from downstream analysis due to failure of the DNA extraction. All other DNA samples were
128 subsequently refrigerated until they were shipped to Génome Québec (Montréal, Quebec, Canada)
129 for library preparation and Illumina sequencing. For samples B2, B3, B5, R1P5, R1P9, R1P14,
130 R3P3, R3P15, R3P20, R3P9-, R3P10-, R3P12- (**Table S1**), library preparation was performed
131 using the NxSeq® AmpFREE Low DNA Library Preparation Kit (Lucigen) using the Xp protocol,
132 as suggested by the manufacturer. These samples were sequenced using 150-bp paired-end
133 technology on an Illumina NovaSeq 6000 instrument. For samples B4, R1P1, R1P18, R3P5,
134 R3P11, R3P14-, R3P18- (**Table S1**), library preparation was performed using the Illumina® DNA
135 PCR-Free Prep, Tagmentation Kit following the manufacturer's recommendations. These samples
136 were likewise sequenced using 150-bp paired-end technology, but on an Illumina NovaSeq X Plus
137 instrument.
138
139 **Taxonomic classification of the raw Illumina reads**
140 Illumina reads were taxonomically classified using Kraken (v2.1.3) (Wood et al. 2019) using a
141 database consisting of the bacteria, archaea, fungi, and virus reference libraries, and post-processed
142 using Bracken (v2.7) (Lu et al. 2017). Alpha diversity and beta diversity measurements were
143 determined based on the species-level output of Bracken. Diversity measurements were
144 determined, analyzed, and visualized in R (v4.5.1) (R Core Team 2025) using the tidyverse
145 (v2.0.0) (Wickham et al. 2019), dplyr (v1.1.4) (Wickham et al. 2018) , phyloseq (v1.52.0)
146 (McMurdie and Holmes 2013), stats (v4.5.1) (R Core Team 2025), ggpubr (v0.6.1) (Kassambara
147 2025), vegan (v2.7.1) (Oksanen et al. 2024), pairwiseAdonis (v0.4.1) (Martinez Arbizu 2017),
148 ggplot2 (v4.0.0) (Wickham 2009), and patchwork (v1.3.2) (Pedersen 2019) packages.

149 KrakenTools (v1.2) (Lu et al. 2022) and KronaTools (v2.8) (Ondov et al. 2011) were used to
150 generate krona plots.
151
152 **Metagenome assembly and binning**
153 Illumina reads were filtered using BBduk (v39.06) (Bushnell 2014) and trimmed using
154 Trimmomatic (v0.39) (Bolger et al. 2014) with the parameters: LEADING:3 TRAILING:3
155 SLIDINGWINDOW:4:15 MINLEN:36. Following trimming, metagenomes were assembled
156 using MEGAHIT (v1.2.9) (Li et al. 2015) with the "presets" option set to "meta-large".
157 Metagenome assembly statistics were calculated using the stats.sh script of BBMap (v37.36)
158 (Bushnell 2014). In addition, to confirm that the alpha and beta diversity metrics were not
159 confounded by differences in sequencing depth, seqtk (v1.3) (https://github.com/lh3/seqtk) was
160 used to filter the trimmed reads to obtain a subset corresponding to 90% of the number of reads
161 from the sample with the fewest reads. These reduced read sets were then used for metagenome
162 assembly using MEGAHIT with the "presets" option set to "meta-large".
163
164 **Assembly of metagenome-assembled genomes**
165 Prior to binning, contigs less than 1500 bp were discarded using pullseq (v1.0.2)
166 (https://github.com/bcthomas/pullseq). Next, an all-against-all mapping of the Illumina reads
167 against each metagenome was performed using bowtie2 (v2.4.5) (Langmead and Salzberg 2012)
168 and sorted using samtools (v1.15.1) (Li et al. 2009). Binning was then performed independently
169 for each sample using MetaBAT2 (v2.14) (Kang et al. 2019), CONCOCT (v1.1.0) (Alneberg et
170 al. 2014), MaxBin2 (v2.2.7) (Wu et al. 2016), and SemiBin2 (v2.1.0) (Pan et al. 2023). From each
171 of the metagenomes, an optimized set of MAGs was produced using DAS_Tool (v1.1.4) (Sieber

172 et al. 2018) and the output of the four binning algorithms. In addition, bins were generated with
173 VAMB (v4.1.3) (Nissen et al. 2021, 20), using all metagenomes and with read mapping performed
174 using minimap2 (v2.24-r1122) (Li 2018). Finally, a non-redundant set of high-quality MAGs (>
175 70% completeness; < 10% contamination) was generated from all the produced MAGs using dRep
176 (v3.4.1) (Olm et al. 2017) and a secondary clustering threshold of 99%. The dependencies for dRep
177 included Mash (v2.3) (Ondov et al. 2016) MUMmer (v4.0.0rc1) (Kurtz et al. 2004), CheckM
178 (v1.2.2) (Parks et al. 2015), Prodigal (v2.6.3) (Hyatt et al. 2010), and pplacer (v1.1.alpha19)
179 (Matsen et al. 2010).
180
181 **Taxonomic classification of the assembled metagenomes**
182 Prior to taxonomic classification, contigs less than 500 bp were discarded using pullseq. Contigs
183 were taxonomically classified using MMSeqs2 (v0a6b8c) (Steinegger and Söding 2017) with the
184 UniRef90 database (downloaded 18 July 2024). Custom scripts were used to convert the MMSeqs2
185 output data into taxa abundance tables, with taxa abundances calculated as the sum of contig length
186 multiplied by contig sequencing depth for all contigs with a given taxonomic classification. Alpha
187 diversity and beta diversity metrics were determined, analyzed, and visualized in R using the
188 tidyverse, ggplot2, dplyr, phyloseq, stats, ggpubr, vegan, pairwiseAdonis, and patchwork
189 packages. The relative abundances of the taxa with an average relative abundance of at least 1.0%
190 were visualized as bubble plots and stacked bar plots with R's ggplot2, patchwork, and
191 randomcoloR (v1.1.0.1) (Ammar 2019) packages. Lastly, the R packages ANCOMBC2 (v2.10.1)
192 (Lin and Peddada 2024) and microbiome (v1.30.0) (Lahti and Shetty 2019) were used to identify
193 statistically significant differences in taxa abundances for taxa with an average relative abundance
194 of at least 0.1% across samples. Differentially abundant taxa were then visualized in R using the

195 pheatmap (v1.0.13) (Kolde 2025) package.

196

197 **Taxonomic classification of metagenome-assembled genomes**

198 MAGs were taxonomically classified using GTDB-Tk (v2.4.0) with the R220 database and the
199 classify_wf workflow (Chaumeil et al. 2020). To construct a phylogeny of the bacterial MAGs,
200 the identify function of GTDB-Tk was used to identify homologs of the bac120 gene set, following
201 which the align function of GTDB-Tk was used to align each marker set and then concatenate the
202 alignments. Lastly, the concatenated alignment was used to construct a maximum likelihood
203 phylogeny using IQ-TREE2 (v2.2.2.4) (Minh et al. 2020). First, ModelFinder (Kalyaanamoorthy
204 et al. 2017), was used to identify the best scoring model based on Bayesian information criterion
205 (BIC). Then, IQ-TREE2 was run using the best-scoring model (LG+F+R5) with branch support
206 assessed using the Shimodaira–Hasegawa-like approximate likelihood ratio test (SH-aLRT) and
207 ultrafast jackknife analysis with a subsampling proportion of 40%, with both metrics calculated
208 from 1,000 replicates. Phylogenies were visualized using iTOL (Letunic and Bork 2024).

209

210 **Characterization of the metabolic potential of the metagenomes and MAGs**

211 Prior to functional annotation, contigs less than 1000 bp were discarded from the metagenomes
212 using pullseq. Next, DRAM (v0.1.2) (Shaffer et al. 2020), as implemented on the KBase platform
213 (Arkin et al. 2018), was used to annotate all metagenomes and MAGs. For the metagenomes, the
214 KEGG annotations were extracted from the annotation file, and a Bray-Curtis distance matrix was
215 produced and visualized using a Principal Coordinate Analysis in R with the ggplot2, dplyr,
216 phyloseq, and patchwork packages. Statistical analyses were performed in R using the vegan and
217 pairwiseAdonis packages. Group specific functional differences were determined and visualized

218 using the dplyr, stats, dunn.test (v1.3.6) (Dinno 2024), and ggplot2 packages.

219 Prior to annotation of BGCs, contigs less than 500 bp were discarded from the
220 metagenomes using pullseq. BGCs were identified in the reduced metagenomes using antiSMASH
221 (v7.0) (Blin et al. 2023) with default parameters, after which BiG-SCAPE (v1.1.8) (Navarro-
222 Muñoz et al. 2020) was run with default parameters to examine BGC diversity across the
223 metagenomes. Likewise, BGCs were identified in the MAGs using antiSMASH and BiG-SCAPE.
224 The output files were processed and visualized as heatmaps in R using the dplyr, ggplot2 and
225 patchwork packages.

226

227 **RESULTS**

228 **Hazelnut rhizosphere sampling**

229 Rhizosphere samples were collected from 15 hazelnut trees situated at Rutgers University Hort
230 Farm 3, East Brunswick, New Jersey, USA, in October 2022. Five samples were collected from
231 each of the following tree types: native *C. americana* plants (henceforth referred to as "native"),
232 *C. avellana* resistant to *A. anomala* (henceforth referred to as "resistant), and susceptible *C.*
233 *avellana* (henceforth referred to as "susceptible"). The *C. americana* plants were derived from
234 open pollinated seeds obtained from wild plants in Dearborn, Michigan, whereas the *C. avellana*
235 plants were the product of a controlled cross of a H4AR21P05 (Jacobs et al. 2024b) female (open
236 pollinated seed from Warsaw, Poland) with a OSU 474.084 ('Lewis' x 'Tonda di Giffoni') x OSU
237 540.084 (a full sibling of 'Sacajawea') male pollen source, obtained from Shawn Mehlenbacher
238 of Oregon State University. These *C. avellana* plants were expected to segregate for a resistance
239 (R) gene originating from Poland (Capik et al., 2013). The two groups of *C. avellana* trees used
240 for this study, therefore, represent full siblings with the resistant group expressing no signs or

241 symptoms of disease and the susceptible expressing obvious signs of infection with pronounced
242 cankers and stem dieback predicated on segregation of the major R gene. At the time of collection,
243 the trees were ~6 years of age and have maintained consistent disease phenotypes for ~8 years as
244 of 2024. All rhizosphere samples were collected from soils adjacent to tree roots, at a depth of ~
245 15 cm and a radius of ~ 15 cm from the trunk of the tree. For comparison, five bulk soil samples
246 (not near tree roots) were also collected from a depth of ~ 15 cm around the orchard; however, the
247 DNA isolation from one bulk soil sample failed, leaving us with four bulk soil samples.
248
249 **Metagenomic sequencing and assembly statistics**
250 Illumina 150 bp paired-end sequencing was used to characterize the microbial community of each
251 of the soil samples, generating between ~ 35 million and ~118 million paired-end reads per sample
252 (**Table S1**), of which between ~ 31 million and ~ 113 million survived quality control (**Table S1**).
253 Metagenome assembly using MEGAHIT resulted in assemblies of 544 Mb to 4007 Mb in size,
254 with N50 values between 446 kb and 2260 kb (**Table S1**). When limiting the metagenomes to
255 contigs of at least 0.5 kb in size, the assemblies averaged 612 Mb and contained an average of
256 768,075 contigs (**Table S1**). Likewise, when limiting the metagenomes to contigs of at least 1 kb
257 in size, the assemblies averaged 187 Mb and contained an average of 115,156 contigs (**Table S1**).
258
259 **Taxonomic characterization of the hazelnut rhizosphere**
260 Initially, the community composition of each rhizosphere and bulk soil sample was evaluated
261 based on the raw Illumina reads using Kraken2 and Bracken, with a database consisting of the
262 bacteria, archaea, fungi, and virus reference libraries. However, the rate of classification by
263 Kraken2 was low, with just 0.80% to 1.77% of reads assigned a taxonomy (**Table S2**).

264 Consequently, we instead used MMSeqs2 with the UniRef90 database, to taxonomically classify
265 the assembled contigs (minimum contig size of 0.5 kb); using this approach, contigs encompassing
266 between 6% and 31% of reads were assigned a taxonomy (**Table S2**). Overall, the metagenomes
267 were dominated by bacteria, with 82% to 96% of reads mapping to the classified contigs
268 corresponding to bacteria, compared to 1.0% to 9.5% and 0.3% to 3.8% for archaea and
269 eukaryotes, respectively.

270 Alpha diversity (Shannon diversity index and Simpson diversity index [1-D]) was
271 calculated from the MMSeqs2 output (**Figures 1A, 1B**). No statistically significant differences
272 were observed between sample groups using either of the diversity measures. However, both
273 diversity metrics displayed a trend of the bulk soil samples having lower diversity than the
274 rhizosphere samples; indeed, statistically significant differences were detected for both diversity
275 metrics when comparing bulk soil versus all rhizosphere samples grouped as a single treatment
276 (Kruskal-Wallis p-value < 0.05 for both metrics). In addition, although not statistically significant,
277 there appeared to be greater between-replicate variance in the diversity metrics for the non-native
278 *C. avellana* compared to native *C. americana* samples, perhaps suggesting that the rhizosphere
279 microbial community of the non-native plants was less stably assembled than that of the native
280 plants.

281 Beta diversity was calculated at the species level using Bray-Curtis dissimilarity (**Figure**
282 **1C**). Statistically significant differences (PERMANOVA p-value < 0.001) in beta diversity were
283 observed between the control and each of the three rhizosphere sample groups, providing support
284 that the rhizosphere samples were correctly collected and were reflective of the rhizosphere
285 community. However, no significant differences were observed between the native, resistant, and
286 susceptible rhizosphere samples, suggesting that plant genotype or disease state had little to no

287 impact on the rhizosphere microbiome at a global level.

288 To ensure that the diversity metrics were not being skewed by differences in read depth,
289 the sequencing reads were subsampled to achieve equivalent read numbers (following QC), after
290 which metagenomes were reassembled and MMSeqs2 rerun. The alpha and beta diversity metrics
291 were then recalculated from these data. This process produced qualitatively similar results for the
292 alpha and beta diversity metrics (**Figure S1**), indicating that the observed diversity values were
293 not heavily skewed by differences in read counts between samples.

294

295 **Differentially abundant taxa**

296 The relative abundances of major taxa were investigated across samples at the phylum and genus
297 levels (**Figures 2 and 3**). Initial, qualitative examination of the data revealed that all samples were
298 dominated by the bacterial phyla *Actinomycetota*, *Pseudomonadota*, and *Acidobacteriota* (**Figure**
299 **2A**). At the genus level, the three most abundant taxa were the common soil bacteria
300 *Bradyrhizobium*, *Gaiella*, and *Nocardioides* (**Figure 3A**). Although the archaea represented only
301 a minority of the metagenomes, the archaeal component was dominated by the phylum
302 *Thermoproteota* (syn. *Nitrosophaerota*) (**Figure 2B**), driven by the abundance of the genera
303 *Nitrososphaera* and "*Candidatus* Nitrosocosmicus" (**Figure 3B**). Lastly, examination of the
304 eukaryotic taxa revealed the phylum Basidiomycota was substantially enriched in the rhizosphere
305 samples relative to the bulk soil control, while the phylum Ascomycota also appeared somewhat
306 enriched in many of the rhizosphere samples (**Figure 2C**). The differential abundance of the
307 phylum Basidiomycota was driven mostly by the genera *Hebeloma*, *Laccaria*, *Galerina*, and
308 *Scleroderma*, while the differential abundance of the phylum Ascomycota was driven mostly by
309 the genus *Morchella* and to a lesser extent the genus *Terfezia* (**Figure 3C**). It is important to note,

310 however, that some unexpected eukaryotic taxa were identified in relatively high abundance, such
311 as the shark genus *Chiloscyllium* (**Figure 3C**). This may be the result of poor taxonomic
312 classification of the eukaryotic contigs and/or the overall low abundance of eukaryotes in the data.
313 Regardless, it does suggest that caution should be taken in interpreting the abundance data for the
314 eukaryotic taxa.

315 Following qualitative assessment of the abundance data, ANCOMBC2 was used for
316 quantitative assessment of differential abundances of the taxa accounting for at least 0.1% of the
317 overall relative abundances of the communities. At the phylum level, the eukaryotic phylum
318 Basidiomycota and the bacterial phylum "*Candidatus* Rokuibacteriota" appeared enriched in all
319 three rhizosphere groups relative to the bulk soil controls with (log2[fold change] ≥ 3.9 and 2.3,
320 for Basidiomycota and "*Candidatus* Rokuibacteriota", respectively; **Figure 2A**). On the other
321 hand, the bacterial phylum *Verrucomicrobiota* appeared underrepresented specifically in the
322 rhizosphere communities of the "resistant" *C. avellana* plants relative to the bulk soil controls
323 (log2[fold change] of -1.2; **Figure 2A**). At the genus level, the three rhizosphere groups were
324 depleted in the bacterial genera *Trebonia* (log2[fold change] ≤ -2.6) and *Actinomadura* (log2[fold
325 change] ≤ -1.3) relative to the bulk soil (**Figure 3D**). Compared to the bulk soil controls, the
326 resistant and susceptible *C. avellana* samples (but not the *C. americana* samples) both had an
327 underrepresentation of the bacterial genera *Actinospica* (log2[fold change] ≤ -1.4), *Occallatibacter*
328 (log2[fold change] ≤ -2.8) and "*Candidatus* Sulfotelmatobacter" (log2[fold change] ≤ -2.9), while
329 the bacterial genus *Rhizobacter* appeared enriched (log2[fold change] ≥ 1.5) (**Figure 3D**). The
330 resistant *C. avellana* samples also appeared depleted in the bacterial genera *Amycolatopsis*
331 (log2[fold change] of -1.2), *Actinocrinis* (log2[fold change] of -1.4), and *Edaphobacter* (log2[fold
332 change] of -1.7) and enriched in *Phycicoccus* (log2[fold change] of 1.3), *Ilumatobacter* (log2[fold

333 change] of 1.9), and *Anatilimnocola* (log2[fold change] of 1.8) relative to the bulk soil (**Figure**
334 **3D**). Lastly, the bacterial genus *Microbacterium* was enriched in the resistant *C. avellana* samples
335 relative to the native variety (log2[fold change] of 2.0) (**Figure 3D**). *Microbacterium* also visually
336 appeared to be enriched in the susceptible *C. avellana* compared to the native variety although this
337 difference was not statistically significant.
338
339 **Functional overview of the metagenomes**
340 DRAM was used for functional annotation of all contigs of at least 1 kb in length, and the relative
341 abundance of genes assigned KEGG annotations were used to construct a PCoA plot using Bray-
342 Curtis dissimilarities as a general overview of the functional differentiation of each sample (**Figure**
343 **4**). Although global differences between samples were detected (PERMANOVA p-value of
344 0.031), no statistically significant differences were noted for any of the pairwise comparisons
345 between sample groups. However, although not statistically significant, there did appear to be a
346 slight trend towards the native *C. americana* and resistant *C. avellana* samples grouping together
347 and separating from the sensitive *C. avellana* and bulk soil. Likewise, no clear differences were
348 noted between sample types when comparing the presence of various functions and pathways
349 related to carbohydrate metabolism, methanogenesis and methanotrophy, nitrogen metabolism,
350 short-chain fatty acid and alcohol conversions, and sulfur metabolism (**Figure S2**). Overall, these
351 results indicate that there was little functional differentiation between the sample types at a global
352 level.
353 In addition, prokaryotic biosynthetic gene clusters (BGCs) were annotated in all
354 metagenome assemblies (limited to contigs of at least 0.5 kb) using the program antiSMASH. BiG-
355 SCAPE was then used to group the antiSMASH annotations based on the class and predicted

356 products of the BGCs (**Figure 5**). The distribution of BGCs across samples was largely similar,
357 regardless of the sample group, with BGCs associated with aryl polyenes, indoles, nonribosomal
358 peptides, phosphonates, ribosomally synthesized and post-translationally modified peptides,
359 polyketides, terpenes, and thioamitides detected across the majority of samples.
360

361 **Reconstruction and characterization of metagenome-assembled genomes**

362 Following dereplication using an average nucleotide identity (ANI) threshold of 99%, 45 high-
363 quality (completeness ≥ 70%, contamination ≤ 10%) metagenome-assembled genomes (MAGs)
364 were constructed from the dataset and taxonomically categorized with GTDB-Tk, including 41
365 bacterial and 4 archaeal MAGs (**Figure 6, Table S3**). Interestingly, only one of the 45 MAGs
366 could be taxonomically classified at the species level when using the Genome Taxonomy Database
367 Toolkit (GTDB-Tk) with database R220, while an additional nine were classified to the genus
368 level. The four archaeal MAGs represent four distinct species from three genera within the family
369 *Nitrososphaeraceae* (phylum *Thermoproteota*). On the other hand, nine phyla are represented
370 amongst the 41 bacterial MAGs, with the majority of MAGs belonging to the phyla
371 *Actinomycetota* (21 MAGs), *Pseudomonadota* (9 MAGs), and *Acidobacteriota* (6 MAGs). MAGs
372 were functionally annotated with DRAM, and a summary of the results are provided as **Figure S3**.
373 In addition, antiSMASH and BiG-SCAPE were used to detect and summarize the abundance of
374 BGCs in the MAGs, and these results are summarized in **Figure S4**.
375

376 **DISCUSSION**

377 **The hazelnut rhizosphere microbiome showed only minor differences compared to bulk soil**

378 Previous studies examining bacterial community structure in the roots of woody plants (*Quercus*,

379 *Populus*, and *Pinus*) found that bacterial community structure was shaped more strongly by host
380 tree species than by soil origin (Bonito et al. 2014). We therefore expected to see differences
381 between the microbial community of the rhizosphere samples compared to the bulk soil samples.
382 As expected, the bulk soil samples were clearly delineated from the rhizosphere samples based on
383 the alpha and beta diversity measures. This differentiation appeared to be mainly driven by changes
384 in the frequencies of low abundance taxa as we observed few differences in the relative abundances
385 of the primary taxa (those with relative abundances ≥ 0.1%). However, the current study examined
386 only a single time point. Considering that another study observed that the prokaryotic component
387 of the maize rhizosphere only differed from bulk soil at specific stages of plant development
388 (Wattenburger et al. 2019), it may be that sampling at a different time of year, or sampling deeper
389 roots, would reveal more dramatic changes in the hazelnut rhizosphere microbial community
390 structure than observed here.

391 Few differences were observed between the microbial communities of the different
392 hazelnut genotypes, contrary to our expectation (Lopes et al. 2023). Likewise, we observed little
393 difference between *C. avellana* plants that were or were not infected with *A. anomala*, despite
394 previous studies observing that foliar pathogens can indirectly impact rhizosphere microbial
395 communities in ways that could potentially have positive impacts on plant disease tolerance
396 (Berendsen et al. 2018; Jiang et al. 2023; Luo et al., 2022; Yang et al. 2020). While these results
397 could suggest that hazelnut genotype and disease status have little impact on the rhizosphere
398 microbiome, it may also be that differences would be more pronounced at other times of the year,
399 or that deeper sequencing and/or taxonomic classification of a higher portion of the contigs would
400 reveal additional differences missed here.

401

402 **Composition of the hazelnut microbial community**

403 We found that the fungal phylum Basidiomycota was enriched in all rhizosphere samples relative
404 to bulk soil. Likewise, the fungal phyla Ascomycota appeared slightly enriched in the rhizosphere
405 samples, although Ascomycota did not meet the 0.1% relative abundance threshold used to retain
406 abundant taxa from the results of ANCOMBC2. Interestingly, a separate study reported
407 Ascomycota, Basidiomycota, and Mortierellomycota as the dominant fungal phyla in the
408 rhizosphere of hazelnut varieties grown in Beijing, China (Ma et al. 2021). Similarly, the phyla
409 Basidiomycota and Ascomycota were the dominant fungal phyla in the rhizosphere of the
410 deciduous shrub *Paeonia ludlowii*, with Basidiomycota being the most dominant in the autumn
411 (Qiao et al. 2023). Overall, the consistency in these results provides support that our rhizosphere
412 samples accurately capture the hazelnut rhizosphere microbiome.

413 Although there is limited data on the effects of bacteria on hazelnut tree health and growth,
414 one study reported that inoculation of *C. avellana* seedlings with the bacteria *Pseudomonas putida*,
415 *B. subtilis*, and *Enterobacter cloacae* can improve growth (Rostamikia et al. 2017). Therefore, we
416 wished to use our metagenomics data to help identify microbes in the hazelnut rhizosphere
417 microbiome that could potentially be targets to develop into biocontrol agents to limit the impact
418 of *A. anomala* infection. To this end, we focused on the microbes that were either enriched or
419 depleted in the hazelnut microbiome. One taxon of particular interest based on the relative and
420 differential abundance data was the bacterial phylum "*Candidatus* Rokuibacteriota", which was
421 enriched in all three rhizosphere groups relative to bulk soil. "*Candidatus* Rokuibacteriota" have
422 large genomes with high GC content, with the capacity for multifaceted mixotrophic metabolism
423 (Becraft et al. 2017). Bacteria from this phylum have also been reported to encode numerous
424 biosynthetic loci in their genomes (Sharrar et al. 2020). Consequently, members of this phylum

425 exhibit characteristics of relevance for biocontrol applications, and we suggest that their utility
426 should be explored within this context.

427 On the other hand, the bacterial genera *Actinospica*, *Occallatibacter*, and "*Candidatus*
428 Sulfotelmatobacter" were depleted in the susceptible and tolerant varieties of *C. avellana* relative
429 to bulk soil, unlike the native *C. americana* variety. *Actinospica* may be of particular note for *A.*
430 *anomala* disease management, as there is an ongoing interest in the efficacy of acidophilic
431 actinomycetes as biocontrol agents against phytopathogenic fungi (Poomthongdee et al. 2015).
432 Supplementing the abundance of this genus in the *C. avellana* microbiome may therefore be a
433 strategy worth exploring for *A. anomala* disease management.

434 In terms of eukaryotic microbes, associations with mycorrhizal fungi have been shown to
435 enhance disease tolerance in woody perennials (Dong et al. 2021; Kebert et al. 2022), and a variety
436 of additional benefits have been described for mycorrhizal associated hazelnut trees. In *C.*
437 *avellana*, association with the ectomycorrhizal forming fungus *Tuber melanosporum* was reported
438 to regulate important plant defense genes, which may favourably impact the host plant's response
439 to stress (Sillo et al. 2022). Inoculation of hybrid hazel (*C. heterophylla* x *C. avellana*) seedlings
440 with the ectomycorrhizal fungus *Scleroderma bovista* was reported to promote growth, enhancing
441 photosynthetic efficiency and total plant weight (Cheng et al. 2024). In addition, inoculation with
442 the arbuscular mycorrhizal fungus *Glomus iranicum* var. *tenuihypharum* was found to increase the
443 number of female flowers and overall yield in the Tonda di Giffoni variety of *C. avellana* by 60%
444 and 38%, respectively, relative to the uninoculated control (Luciani et al. 2019). In our study, the
445 fungal genera *Hebeloma*, *Galerina*, *Laccaria*, *Morchella*, *Terfezia*, and *Scleroderma* appeared
446 enriched in the three groups of rhizosphere samples, relative to the control group; however, as the
447 overall relative abundance of fungi across samples was generally low, most of these taxa did not

448 meet the 0.1% relative abundance threshold required to be retained in the results from
449 ANCOMBC2. Isolates of species from these fungal taxa from the hazelnut rhizosphere may
450 therefore represent interesting candidates to explore for plant growth promotion and/or biocontrol
451 against *A. anomala* in North America.
452
453 **Primary metabolism of the hazelnut rhizosphere microbiome**
454 Rhizosphere microbes play important roles in nutrient cycling and availability (Thepbandit and
455 Athinuwat 2024) and consequently, they can impact plant nutrition and thus disease tolerance. For
456 example, nitrogen availability can impact both physical and biochemical defence mechanisms in
457 plants, yet the consequences of enhanced endogenous nitrogen can be difficult to anticipate, as
458 they may be favourable or detrimental to plant pathogen tolerance depending on context (Sun et
459 al. 2020). In our study, global differences in the KEGG metabolic annotations (PERMANOVA p-
460 value of 0.031) were observed between samples, however no pairwise differences were detected
461 between sample groups.
462 Pathways involved in nitrogen metabolism were well represented across most samples
463 including ammonia oxidation, conversion of nitrate to nitrite, nitrite to nitrate, nitrite to nitric
464 oxide, and nitric oxide to nitrous oxide. Though less common, some bulk soil and rhizosphere
465 samples possessed the capacity for nitrite reduction to ammonia. As nitrate serves as the major
466 source of nitrogen for most land plants in aerobic soils (Ho and Tsay 2010), the presence of
467 pathways involved in the production of nitrate across samples highlights the capacity of microbes
468 within these systems to facilitate the production of bioavailable nitrogen for hazelnut. Bioavailable
469 sulfur can also have drastic impacts on plant disease outcomes. For example, inorganic sulfate
470 salts can significantly enhance the resistance of plants to certain fungal pathogens, through a

471 process deemed sulfur-induced resistance (SIR) (Künstler et al. 2020). Here, pathways responsible
472 for the conversion of thiosulfate to sulfate were well represented across all samples besides one of
473 the Susceptible samples. As both bioavailable nitrogenous and sulfur-containing compounds have
474 been demonstrated to alter plant disease tolerance (Bloem et al. 2015; Mur et al. 2017) the
475 application of certain microbial communities that alter the abundance of bioavailable forms of
476 these compounds within the soil may be explored as an alternative means of broadly improving
477 plant health.

478 Many of the MAGs generated in this study, particularly those within the orders *Gaiellales*
479 and *Hyphomicrobiales* (syn. *Rhizobiales*), encoded pathways involved in the conversion of nitrite
480 to nitric oxide (NO). NO can be generated endogenously in plants and performs important
481 functions in various physiological responses and developmental stages (Hancock 2020; Sun et al.
482 2021), with roles in plant tolerance to abiotic and biotic stress (Fancy et al. 2017, 201; Mur et al.
483 2017). Exogenous application of NO, through the use of NO donors, has been shown to improve
484 plant disease tolerance in several instances (Nasir et al. 2020; Khan et al. 2021; Bakhoum et al.
485 2023). Furthermore, studies suggest that leveraging NO-producing organisms to enhance disease
486 tolerance in plants is a promising avenue to explore. For example, a study examining tomato
487 infected with *Ralstonia solanacearum* found that *Pseudomonas fluorescens* strains overproducing
488 NO displayed better biocontrol efficacy than those that do not overproduce NO (Wang et al. 2005).
489 Consequently, it would be interesting to isolate diverse strains from promising genera within the
490 *Gaiellales* and *Hyphomicrobiales* orders, which we found commonly encode the pathways for NO
491 production, and assess them for their impact on hazelnut disease tolerance. Of particularly interest
492 would be isolates that additionally have the potential to convert thiosulfate to sulfate.
493

494 **Secondary metabolism of the hazelnut rhizosphere microbiome**

495 Soil microbes represent a rich source of secondary metabolites (Sharrar et al. 2020) that perform
496 diverse functions in ecological systems and can mediate symbioses between microbes and plants
497 in certain contexts (Demain and Fang 2000) and ameliorate biotic stress in plants (Ruparelia et al.
498 2022). Analyzing the biosynthetic gene clusters (BGCs) involved in the production of secondary
499 metabolites within the hazelnut rhizosphere, therefore, provides an opportunity to identify
500 compounds and microbial taxa that can be screened as biological control agents in hazelnut.

501 In our study, no substantial differences in the distribution of BGC classes were evident
502 between conditions, and all conditions had BGCs encoding the production of non-ribosomal
503 peptides (NRPs), ribosomally synthesized and post-translationally modified peptides (RiPPs), and
504 terpenes. The production of secondary metabolites of these classes has repeatedly been shown to
505 contribute to the biocontrol potential of plant growth-promoting rhizobacteria (PGPRs). For
506 example, *Bacillus* species produce NRPs that can serve as biocontrol agents, such as iturin,
507 surfactin, and fengycin (Ranjan et al. 2023). Likewise, species of the fungal genus *Trichoderma*
508 have demonstrated potential as biocontrol agents (Sood et al. 2020), which could relate to the
509 diversity of terpenoids and complex terpenes produced by these organisms (Bai et al. 2022; Lee et
510 al. 2016).

511 Many of the MAGs assembled in this study have the genetic potential to produce diverse
512 secondary metabolites. One such example is MAG-30, classified as belonging to the species
513 "*Lysobacter yananisis*". Species of the genus *Lysobacter* have potential as biocontrol agents
514 (Kilic-Ekici and Yuen 2003; Puopolo et al. 2014), and they produce a range of antibiotics active
515 against numerous plant pathogens (Gómez Expósito et al. 2015; Hayward et al. 2010). Likewise,
516 our *Lysobacter* MAG has the genetic potential to produce various secondary metabolites of

517 relevance for biocontrol, including NRPs, lantipeptides, polyketides, and RiPPs. Another MAG
518 with high biosynthetic potential is MAG-07, classified as belonging to the genus *Actinospica*.
519 Species of this genus have been isolated from diverse ecosystems including forest soils (Kusuma
520 et al. 2022; Cavaletti et al. 2006), and studies suggest that members of this genus have strong
521 biocontrol potential (Qi et al. 2019; Rodriguez-Mena et al. 2022). Indeed, members of the genus
522 *Actinospica* have high genetic potential to produce a wide array of secondary metabolites (Majer
523 et al. 2021). Likewise, our *Actinospica* MAG contains several genomic regions potentially
524 involved in the production of NRPs, lantipeptides, RIPPs, polyketides, and terpenes. Considering
525 these results, it would be interesting to isolate strains of the genera *Lysobacter* and *Actinospica*
526 from hazelnut rhizosphere soils and investigate their potential to serve as biocontrol strains and
527 reduce the susceptibility of hazelnut to *A. anomala* infection.
528

529 **Conclusions**

530 The co-evolution of plants and their resident microbial communities has resulted in a complex
531 dynamic where the microbial genetic complement can drastically impact important plant features.
532 Soil microbes participate in important biogeochemical cycles that impact plant nutrient
533 acquisition, while plant-associated microbes can also influence plant immunity. Here,
534 metagenomics was used to examine the microbial communities of three hazelnut rhizosphere
535 sample groups obtained from trees that displayed differing levels of resistance to the pathogen *A.*
536 *anomala*: *C. americana* (resistant), *C. avellana* (susceptible) and *C. avellana* (resistant). While the
537 rhizosphere samples were differentiated from the bulk soil samples, little taxonomic or functional
538 variation was seen between the different rhizosphere groups. A total of 45 dereplicated, high-
539 quality MAGs were generated, many of which carried multiple BGCs. This included two MAGs

540 representing organisms from the bacterial genera *Actinospica* and *Lysobacter* that have previously
541 been identified as potential biocontrol agents. This study serves to inform future efforts aimed at
542 leveraging hazelnut-associated microbes toward the improvement of diverse hazelnut features
543 including disease outcomes, identifying promising candidate taxa that could be isolated and
544 screened for their capacity to manage *A. anomala* infection. In addition, this study provides
545 insights into the taxonomic diversity and functional potential of the rhizosphere microbial
546 communities of hazelnut, expanding our understanding of the rhizosphere microbiome of woody
547 perennials.
548
549 **Data availability**
550 All raw Illumina sequencing data, metagenome assemblies, and MAGs are available from the
551 National Center for Biotechnology Information (NCBI) under BioProject PRJNA1338491
552 Accessions for individual datasets are provided in **Table S3**. All code to repeat the analyses
553 described in this manuscript is available through GitHub (github.com/diCenzo-
554 Lab/016_2025_hazelnut_rhizosphere_metagenomics).
555
556 **ACKNOWLEDGEMENTS**
557 We thank Sharen Roland and other personnel at the Centre d'Expertise et de Services (CES) of
558 Génome Québec for the advice on sequencing strategies and for performing all the Illumina
559 sequencing reported in this study. We would also like to thank Rutgers University Department of
560 Plant Biology for providing access to their facilities for sample collection and preparation. This
561 work was funded by the Natural Sciences and Engineering Research Council of Canada (NSERC)
562 through Discovery Grants to S.R. and G.C.D. and the NSERC Collaborative Research and

563 Training Experience Grant "Genome Editing for Food Security and Environmental Sustainability"
564 to S.R. This work was also supported by the USDA-NIFA Hatch project NJ12171 through the
565 New Jersey Agricultural Experiment Station. This research was enabled, in part, through
566 computational resources provided by Compute Ontario (computeontario.ca) and the Digital
567 Research Alliance of Canada (alliancecan.ca).

568

569 **REFERENCES**

570 Ali, I., Sultan, T., Subhan, F., Haleem, K. S., Sultana, N., and Tauseef, I. 2018. PGPRs of plum
571 (*Prunus domestica*) rhizosphere enhance plant growth and antagonize fungal activity in
572 vitro. **Acta Agric. Scand. Sect. B — Soil Plant Sci.** 68:367–378.
573 https://doi.org/10.1080/09064710.2017.1410565.

574 Alneberg, J., Bjarnason, B. S., de Bruijn, I., Schirmer, M., Quick, J., Ijaz, U. Z., Lahti, L., Loman,
575 N. J., Andersson, A. F., and Quince, C. 2014. Binning metagenomic contigs by coverage and
576 composition. **Nat. Methods** 11:1144–1146. https://doi.org/10.1038/nmeth.3103.

577 Ammar, R. 2019. **randomcoloR: generate attractive random colors.** https://CRAN.R-
578 project.org/package=randomcoloR.

579 Arkin, A. P., Cottingham, R. W., Henry, C. S., Harris, N. L., Stevens, R. L., Maslov, S., Dehal, P.,
580 Ware, D., Perez, F., Canon, S., Sneddon, M. W., Henderson, M. L., Riehl, W. J., Murphy-
581 Olson, D., Chan, S. Y., Kamimura, R. T., Kumari, S., Drake, M. M., Brettin, T. S., Glass, E.
582 M., Chivian, D., Gunter, D., Weston, D. J., Allen, B. H., Baumohl, J., Best, A. A., Bowen,
583 B., Brenner, S. E., Bun, C. C., Chandonia, J.-M., Chia, J.-M., Colasanti, R., Conrad, N.,
584 Davis, J. J., Davison, B. H., DeJongh, M., Devoid, S., Dietrich, E., Dubchak, I., Edirisinghe,
585 J. N., Fang, G., Faria, J. P., Frybarger, P. M., Gerlach, W., Gerstein, M., Greiner, A.,

586 Gurtowski, J., Haun, H. L., He, F., Jain, R., Joachimiak, M. P., Keegan, K. P., Kondo, S.,
587 Kumar, V., Land, M. L., Meyer, F., Mills, M., Novichkov, P. S., Oh, T., Olsen, G. J., Olson,
588 R., Parrello, B., Pasternak, S., Pearson, E., Poon, S. S., Price, G. A., Ramakrishnan, S.,
589 Ranjan, P., Ronald, P. C., Schatz, M. C., Seaver, S. M. D., Shukla, M., Sutormin, R. A., Syed,
590 M. H., Thomason, J., Tintle, N. L., Wang, D., Xia, F., Yoo, H., Yoo, S., and Yu, D. 2018.
591 KBase: The United States Department of Energy Systems Biology Knowledgebase. **Nat.**
592 **Biotechnol.** 36:566–569. https://doi.org/10.1038/nbt.4163.
593 Bai, B., Liu, C., Zhang, C., He, X., Wang, H., Peng, W., and Zheng, C. 2022. *Trichoderma* species
594 from plant and soil: an excellent resource for biosynthesis of terpenoids with versatile
595 bioactivities. **J. Adv. Res.** 49:81–102. https://doi.org/10.1016/j.jare.2022.09.010.
596 Bakhoum, G. Sh., Sadak, M. Sh., and Thabet, M. S. 2023. Induction of tolerance in groundnut
597 plants against drought stress and *Cercospora* leaf spot disease with exogenous application
598 of arginine and sodium nitroprusside under field conditions. **J. Soil Sci. Plant Nutr.**
599 23:6612–6631. https://doi.org/10.1007/s42729-023-01514-x.
600 Bakker, P. A. H. M., Berendsen, R. L., Doornbos, R. F., Wintermans, P. C. A., and Pieterse, C. M.
601 J. 2013a. The rhizosphere revisited: root microbiomics. **Front. Plant Sci.** 4.
602 https://doi.org/10.3389/fpls.2013.00165.
603 Bakker, P. A. H. M., Doornbos, R. F., Zamioudis, C., Berendsen, R. L., and Pieterse, C. M. J.
604 2013b. Induced systemic resistance and the rhizosphere microbiome. **Plant Pathol. J.**
605 29:136–143. https://doi.org/10.5423/PPJ.SI.07.2012.0111.
606 Becraft, E. D., Woyke, T., Jarett, J., Ivanova, N., Godoy-Vitorino, F., Poulton, N., Brown, J. M.,
607 Brown, J., Lau, M. C. Y., Onstott, T., Eisen, J. A., Moser, D., and Stepanauskas, R. 2017.
608 Rokubacteria: genomic giants among the uncultured bacterial phyla. **Front. Microbiol.** 8.

609 https://doi.org/10.3389/fmicb.2017.02264.

610 Berdeni, D., Cotton, T. E. A., Daniell, T. J., Bidartondo, M. I., Cameron, D. D., and Evans, K. L.
611 2018. The effects of arbuscular mycorrhizal fungal colonization on nutrient status, growth,
612 productivity, and canker resistance of apple (*Malus pumila*). **Front. Microbiol.** 9:1461.
613 https://doi.org/10.3389/fmicb.2018.01461.

614 Berendsen, R. L., Pieterse, C. M. J., and Bakker, P. A. H. M. 2012. The rhizosphere microbiome
615 and plant health. **Trends Plant Sci.** 17:478–486.
616 https://doi.org/10.1016/j.tplants.2012.04.001.

617 Berendsen, R. L., Vismans, G., Yu, K., Song, Y., de Jonge, R., Burgman, W. P., Burmølle, M.,
618 Herschend, J., Bakker, P. A. H. M., and Pieterse, C. M. J. 2018. Disease-induced assemblage
619 of a plant-beneficial bacterial consortium. **ISME J.** 12:1496–1507.
620 https://doi.org/10.1038/s41396-018-0093-1.

621 Blin, K., Shaw, S., Augustijn, H. E., Reitz, Z. L., Biermann, F., Alanjary, M., Fetter, A., Terlouw,
622 B. R., Metcalf, W. W., Helfrich, E. J. N., van Wezel, G. P., Medema, M. H., and Weber, T.
623 2023. antiSMASH 7.0: new and improved predictions for detection, regulation, chemical
624 structures and visualization. **Nucleic Acids Res.** 51:W46–W50.
625 https://doi.org/10.1093/nar/gkad344.

626 Bloem, E., Haneklaus, S., and Schnug, E. 2015. Milestones in plant sulfur research on sulfur-
627 induced-resistance (SIR) in Europe. **Front. Plant Sci.** 5.
628 https://doi.org/10.3389/fpls.2014.00779.

629 Boccacci, P., and Botta, R. 2009. Investigating the origin of hazelnut (*Corylus avellana* L.)
630 cultivars using chloroplast microsatellites. **Genet. Resour. Crop Evol.** 56:851–859.
631 https://doi.org/10.1007/s10722-009-9406-6.

632 Bolger, A. M., Lohse, M., and Usadel, B. 2014. Trimmomatic: a flexible trimmer for Illumina
633 sequence data. **Bioinformatics** 30:2114–2120.
634 https://doi.org/10.1093/bioinformatics/btu170.
635 Bonito, G., Reynolds, H., Robeson II, M. S., Nelson, J., Hodkinson, B. P., Tuskan, G., Schadt, C.
636 W., and Vilgalys, R. 2014. Plant host and soil origin influence fungal and bacterial
637 assemblages in the roots of woody plants. **Mol. Ecol.** 23:3356–3370.
638 https://doi.org/10.1111/mec.12821.
639 Bouffaud, M., Poirier, M., Muller, D., and Moënne-Loccoz, Y. 2014. Root microbiome relates to
640 plant host evolution in maize and other Poaceae. **Environ. Microbiol.** 16:2804–2814.
641 https://doi.org/10.1111/1462-2920.12442.
642 Bushnell, B. 2014. BBMap: a fast, accurate, splice-aware aligner.
643 https://www.osti.gov/biblio/1241166.
644 Capik, J. M., Muehlbauer, M., Novy, A., Honig, J. A., & Molnar, T. J. 2013. Eastern Filbert Blight-
645 resistant hazelnuts from Russia, Ukraine, and Poland. **HortScience** 48:466–
646 473. https://doi.org/10.21273/HORTSCI.48.4.466.
647 Cavaletti, L., Monciardini, P., Schumann, P., Rohde, M., Bamonte, R., Busti, E., Sosio, M., and
648 Donadio, S. 2006. *Actinospica robiniae* gen. nov., sp. nov. and *Actinospica acidiphila* sp.
649 nov.: proposal for *Actinospicaceae* fam. nov. and *Catenulisporinae* subord. nov. in the order
650 *Actinomycetales*. **Int. J. Syst. Evol. Microbiol.** 56:1747–1753.
651 https://doi.org/10.1099/ijs.0.63859-0.
652 Chaumeil, P.-A., Mussig, A. J., Hugenholtz, P., and Parks, D. H. 2020. GTDB-Tk: a toolkit to
653 classify genomes with the Genome Taxonomy Database. **Bioinformatics** 36:1925–1927.
654 https://doi.org/10.1093/bioinformatics/btz848.

655 Cheng, Y., Sun, S., Lou, H., Dong, Y., He, H., Mei, Q., and Liu, J. 2024. The ectomycorrhizal
656 fungus *Scleroderma bovista* improves growth of hazelnut seedlings and plays a role in auxin
657 signaling and transport. **Front. Microbiol**. 15. https://doi.org/10.3389/fmicb.2024.1431120.
658 Demain, A. L., and Fang, A. 2000. The natural functions of secondary metabolites. **Adv. Biochem.**
659 **Eng. Biotechnol.** 69:1–39. https://doi.org/10.1007/3-540-44964-7_1.
660 Derikvand, F., Bazgir, E., El Jarroudi, M., Darvishnia, M., Mirzaei Najafgholi, H., Laasli, S.-E.,
661 and Lahlali, R. 2023. Unleashing the potential of bacterial isolates from apple tree
662 rhizosphere for biocontrol of *Monilinia laxa*: a promising approach for combatting brown
663 rot disease. **J. Fungi** 9:828. https://doi.org/10.3390/jof9080828.
664 Dinno, A. 2024. **dunn.test: dunn's test of multiple comparisons using rank sums**.
665 https://CRAN.R-project.org/package=dunn.test.
666 Dlamini, S. P., Akanmu, A. O., and Babalola, O. O. 2022. Rhizospheric microorganisms: the
667 gateway to a sustainable plant health. **Front. Sustain. Food Syst.** 6:925802.
668 https://doi.org/10.3389/fsufs.2022.925802.
669 Dong, F., Wang, Y., and Tang, M. 2021. Effects of *Laccaria bicolor* on gene expression of *Populus*
670 *trichocarpa* root under poplar canker stress**. J. Fungi** 7:1024.
671 https://doi.org/10.3390/jof7121024.
672 Dordas, C. 2008. Role of nutrients in controlling plant diseases in sustainable agriculture. A review.
673 **Agron. Sustain. Dev.** 28:33–46. https://doi.org/10.1051/agro:2007051.
674 Dotaniya, M. L., and Meena, V. D. 2015. Rhizosphere effect on nutrient availability in soil and its
675 uptake by plants: a review. **Proc. Natl. Acad. Sci. India Sect. B Biol. Sci.** 85:1–12.
676 https://doi.org/10.1007/s40011-013-0297-0.
677 Ezrari, S., Mhidra, O., Radouane, N., Tahiri, A., Polizzi, G., Lazraq, A., and Lahlali, R. 2021.

678 Potential role of rhizobacteria isolated from citrus rhizosphere for biological control of citrus
679 dry root rot. **Plants Basel Switz.** 10:872. https://doi.org/10.3390/plants10050872.
680 Fancy, N. N., Bahlmann, A.-K., and Loake, G. J. 2017. Nitric oxide function in plant abiotic stress.
681 **Plant Cell Environ.** 40:462–472. https://doi.org/10.1111/pce.12707.
682 Fitzpatrick, C. R., Copeland, J., Wang, P. W., Guttman, D. S., Kotanen, P. M., and Johnson, M. T.
683 J. 2018. Assembly and ecological function of the root microbiome across angiosperm plant
684 species. **Proc. Natl. Acad. Sci.** 115:E1157–E1165.
685 https://doi.org/10.1073/pnas.1717617115.
686 Food and Agricultural Organization of the United Nations. 2021. **FAOSTAT**.
687 https://www.fao.org/faostat/en/#data/QCL [Accessed 15 Oct. 2024]
688 Gómez Expósito, R., Postma, J., Raaijmakers, J. M., and De Bruijn, I. 2015. Diversity and activity
689 of *Lysobacter* species from disease suppressive soils. **Front. Microbiol.** 6:1243.
690 https://doi.org/10.3389/fmicb.2015.01243.
691 Gupta, R., Anand, G., Gaur, R., and Yadav, D. 2021. Plant–microbiome interactions for sustainable
692 agriculture: a review. **Physiol. Mol. Biol. Plants** 27:165–179.
693 https://doi.org/10.1007/s12298-021-00927-1.
694 Hakim, S., Naqqash, T., Nawaz, M. S., Laraib, I., Siddique, M. J., Zia, R., Mirza, M. S., and Imran,
695 A. 2021. Rhizosphere engineering with plant growth-promoting microorganisms for
696 agriculture and ecological sustainability. **Front. Sustain. Food Syst.** 5:617157.
697 https://doi.org/10.3389/fsufs.2021.617157.
698 Hancock, J. T. 2020. Nitric oxide signaling in plants. **Plants** 9:1550.
699 https://doi.org/10.3390/plants9111550.
700 Hassani, M. A., Durán, P., and Hacquard, S. 2018. Microbial interactions within the plant

701 holobiont. **Microbiome** 6:58. https://doi.org/10.1186/s40168-018-0445-0.

702 Hayward, A. C., Fegan, N., Fegan, M., and Stirling, G. R. 2010. *Stenotrophomonas* and
703 *Lysobacter*: ubiquitous plant-associated gamma-proteobacteria of developing significance in
704 applied microbiology. **J. Appl. Microbiol.** 108:756–770. https://doi.org/10.1111/j.1365-
705 2672.2009.04471.x.

706 Helmstetter, A. J., Oztolan-Erol, N., Lucas, S. J., and Buggs, R. J. A. 2020. Genetic diversity and
707 domestication of hazelnut (*Corylus avellana* L.) in Turkey. **Plants, People, Planet** 2:326–
708 339. https://doi.org/10.1002/ppp3.10078.

709 Ho, C. H., and Tsay, Y. F. 2010. Nitrate, ammonium, and potassium sensing and signaling. **Curr.**
710 **Opin. Plant Biol.** 13:604–610. https://doi.org/10.1016/j.pbi.2010.08.005.

711 Hyatt, D., Chen, G.-L., LoCascio, P. F., Land, M. L., Larimer, F. W., and Hauser, L. J. 2010.
712 Prodigal: prokaryotic gene recognition and translation initiation site identification. **BMC**
713 **Bioinformatics** 11:119. https://doi.org/10.1186/1471-2105-11-119.

714 Jacobs, D. C., Revord, R. S., Capik, J. M., Mehlenbacher, S. A., and Molnar, T. J. 2024a. Variable
715 response of eastern filbert blight resistance sources in New Jersey. **Front. Plant Sci.** 15.
716 https://doi.org/10.3389/fpls.2024.1419265.

717 Jacobs, D. C., Revord, R. S., Capik, J. M., and Molnar, T. J. 2024b. Eastern filbert blight
718 resistant *Corylus avellana* identified from 20 years of germplasm introduction and
719 evaluation at Rutgers University, New Jersey, USA. **Front. Plant Sci.** 15.
720 https://doi.org/10.3389/fpls.2024.1502392.

721 Jeger, M., Bragard, C., Caffier, D., Candresse, T., Chatzivassiliou, E., Dehnen-Schmutz, K.,
722 Gilioli, G., Grégoire, J., Jaques Miret, J. A., MacLeod, A., Navajas Navarro, M., Niere, B.,
723 Parnell, S., Potting, R., Rafoss, T., Rossi, V., Urek, G., Van Bruggen, A., Van der Werf, W.,

West, J., Winter, S., Boberg, J., Gonthier, P., and Pautasso, M. 2018. Pest categorization of *Anisogramma anomala*. **EFSA J.** 16:e05184. https://doi.org/10.2903/j.efsa.2018.5184.

Jiang, H., Xu, X., Fang, Y., Ogunyemi, S. O., Ahmed, T., Li, X., Yang, Y., Yan, C., Chen, J., and Li, B. 2023. Metabarcoding reveals response of rice rhizosphere bacterial community to rice bacterial leaf blight. **Microbiol. Res.** 270:127344. https://doi.org/10.1016/j.micres.2023.127344.

Jones, D. L., and Hinsinger, P. 2008. The rhizosphere: complex by design. **Plant Soil** 312:1–6. https://doi.org/10.1007/s11104-008-9774-2.

Kalyaanamoorthy, S., Minh, B. Q., Wong, T. K. F., von Haeseler, A., and Jermiin, L. S. 2017. ModelFinder: fast model selection for accurate phylogenetic estimates. **Nat. Methods** 14:587–589. https://doi.org/10.1038/nmeth.4285.

Kang, D. D., Li, F., Kirton, E., Thomas, A., Egan, R., An, H., and Wang, Z. 2019. MetaBAT 2: an adaptive binning algorithm for robust and efficient genome reconstruction from metagenome assemblies. **PeerJ.** 7:e7359. https://doi.org/10.7717/peerj.7359.

Kassambara, A. 2025. **ggpubr: 'ggplot2' based publication ready plots**. https://CRAN.R-project.org/package=ggpubr.

Kebert, M., Kostić, S., Zlatković, M., Stojnic, S., Čapelja, E., Zorić, M., Kiprovski, B., Budakov, D., and Orlović, S. 2022. Ectomycorrhizal fungi modulate biochemical response against powdery mildew disease in *Quercus robur* L. **Forests** 13:1491. https://doi.org/10.3390/f13091491.

Khan, M., Al Azawi, T. N. I., Pande, A., Mun, B.-G., Lee, D.-S., Hussain, A., Lee, B.-H., and Yun, B.-W. 2021. The role of nitric oxide-induced ATILL6 in growth and disease resistance in *Arabidopsis thaliana*. **Front. Plant Sci.** 12. https://doi.org/10.3389/fpls.2021.685156.

747 Kilic-Ekici, O., and Yuen, G. Y. 2003. Induced resistance as a mechanism of biological control by
748 *Lysobacter enzymogenes* strain C3**.** **Phytopathology** 93:1103–1110.
749 https://doi.org/10.1094/PHYTO.2003.93.9.1103.
750 Kolde, R. 2025. **pheatmap: Pretty Heatmaps**.
751 https://doi.org/10.32614/CRAN.package.pheatmap.
752 Künstler, A., Gullner, G., Ádám, A. L., Kolozsváriné Nagy, J., and Király, L. 2020. The versatile
753 roles of sulfur-containing biomolecules in plant defense—a road to disease resistance. **Plants**
754 9:1705. https://doi.org/10.3390/plants9121705.
755 Kurtz, S., Phillippy, A., Delcher, A. L., Smoot, M., Shumway, M., Antonescu, C., and Salzberg, S.
756 L. 2004. Versatile and open software for comparing large genomes. **Genome Biol.** 5:R12.
757 https://doi.org/10.1186/gb-2004-5-2-r12.
758 Kusuma, A. B., Putra, K. E., Vanggy, L. R., Loh, J., Nouioui, I., and Goodfellow, M. 2022.
759 *Actinospica acidithermotolerans* sp. nov., a novel actinomycete isolated from sediment from
760 an Indonesian hot spring. **Arch. Microbiol.** 204:518. https://doi.org/10.1007/s00203-022-
761 03058-7.
762 Lahti, L., and Shetty, S. 2019. **microbiome R package**. http://microbiome.github.io
763 Langmead, B., and Salzberg, S. L. 2012. Fast gapped-read alignment with Bowtie 2. **Nat. Methods**
764 9:357–359. https://doi.org/10.1038/nmeth.1923.
765 Lee, S., Yap, M., Behringer, G., Hung, R., and Bennett, J. W. 2016. Volatile organic compounds
766 emitted by *Trichoderma* species mediate plant growth. **Fungal Biol. Biotechnol.** 3:7.
767 https://doi.org/10.1186/s40694-016-0025-7.
768 Lei, S., Xu, X., Cheng, Z., Xiong, J., Ma, R., Zhang, L., Yang, X., Zhu, Y., Zhang, B., and Tian, B.
769 2019. Analysis of the community composition and bacterial diversity of the rhizosphere

770 microbiome across different plant taxa. **MicrobiologyOpen** 8:e00762.
771 https://doi.org/10.1002/mbo3.762.
772 Letunic, I., and Bork, P. 2024. Interactive Tree of Life (iTOL) v6: recent updates to the
773 phylogenetic tree display and annotation tool. **Nucleic Acids Res.** 52:W78–W82.
774 https://doi.org/10.1093/nar/gkae268.
775 Li, D., Liu, C. M., Luo, R., Sadakane, K., and Lam, T.-W. 2015. MEGAHIT: an ultra-fast single-
776 node solution for large and complex metagenomics assembly via succinct de Bruijn graph.
777 **Bioinformatics** 31:1674–1676. https://doi.org/10.1093/bioinformatics/btv033.
778 Li, H. 2018. Minimap2: pairwise alignment for nucleotide sequences. **Bioinformatics** 34:3094–
779 3100. https://doi.org/10.1093/bioinformatics/bty191.
780 Li, H., Handsaker, B., Wysoker, A., Fennell, T., Ruan, J., Homer, N., Marth, G., Abecasis, G.,
781 Durbin, R., and 1000 Genome Project Data Processing Subgroup. 2009. The sequence
782 alignment/map format and SAMtools. **Bioinformatics** 25:2078–2079.
783 https://doi.org/10.1093/bioinformatics/btp352.
784 Li, Z., Li, J., Liu, G., Li, Y., Wu, X., Liang, J., Wang, Z., Chen, Q., and Peng, F. 2025. Isolation,
785 characterization and growth-promoting properties of phosphate-solubilizing bacteria (PSBs)
786 derived from peach tree rhizosphere. **Microorganisms** 13:718.
787 https://doi.org/10.3390/microorganisms13040718.
788 Lin, H., and Peddada, S. D. 2024. Multigroup analysis of compositions of microbiomes with
789 covariate adjustments and repeated measures. **Nat. Methods** 21:83–91.
790 https://doi.org/10.1038/s41592-023-02092-7.
791 Liu, F., Hewezi, T., Lebeis, S. L., Pantalone, V., Grewal, P. S., and Staton, M. E. 2019. Soil
792 indigenous microbiome and plant genotypes cooperatively modify soybean rhizosphere

793 microbiome assembly. **BMC Microbiol.** 19:201. https://doi.org/10.1186/s12866-019-1572-
794 x.
795 Liu, H., Li, J., Carvalhais, L. C., Percy, C. D., Prakash Verma, J., Schenk, P. M., and Singh, B. K.
796 2021. Evidence for the plant recruitment of beneficial microbes to suppress soil-borne
797 pathogens. **New Phytol.** 229:2873–2885. https://doi.org/10.1111/nph.17057.
798 Liu, L., Ma, L., Zhu, M., Liu, B., Liu, X., and Shi, Y. 2023b. Rhizosphere microbial community
799 assembly and association networks strongly differ based on vegetation type at a local
800 environment scale. **Front. Microbiol.** 14:1129471.
801 https://doi.org/10.3389/fmicb.2023.1129471.
802 Liu, S., Tao, C., Zhang, L., Wang, Z., Xiong, W., Xiang, D., Sheng, O., Wang, J., Li, R., Shen, Z.,
803 Li, C., Shen, Q., and Kowalchuk, G. A. 2023a. Plant pathogen resistance is mediated by
804 recruitment of specific rhizosphere fungi. **ISME J.** 17:931–942.
805 https://doi.org/10.1038/s41396-023-01406-z.
806 Lopes, A. C. de A., Mendes, L. W., Brito, K. A. da S. B., da Silva, J. L., Rocha, S. M. B., Antunes,
807 J. E. L., Oliveira, L. M. de S., Melo, V. M. M., Oliveira, F. A. S., Pereira, A. P. de A., Costa,
808 G. do N., da Silva, V. B., Gomes, R. L. F., de Alcantara Neto, F., and Araujo, A. S. F. 2023.
809 Rhizospheric microbial community in plant species from the *Phaseolus* genus. **Appl. Soil**
810 **Ecol.** 182:104731. https://doi.org/10.1016/j.apsoil.2022.104731.
811 Lotfi, N., Soleimani, A., Çakmakçı, R., Vahdati, K., and Mohammadi, P. 2022. Characterization of
812 plant growth-promoting rhizobacteria (PGPR) in Persian walnut associated with drought
813 stress tolerance. **Sci. Rep.** 12:12725. https://doi.org/10.1038/s41598-022-16852-6.
814 Lu, J., Breitwieser, F., Thielen, P., and Salzberg, S. 2017. Bracken: estimating species abundance
815 in metagenomics data. **PeerJ Comput. Sci.** 3:e104. https://doi.org/10.7717/peerj-cs.104.

816 Lu, J., Rincon, N., Wood, D. E., Breitwieser F. P., Pockrandt, C., Langmead, B., Salzberg S. L.,
817 Steinegger, M. 2022. Metagenome analysis using the Kraken software suite. **Nat**
818 **Protoc.** 17:2815–2839. https://doi.org/10.1038/s41596-022-00738-y.
819 Luciani, E., Palliotti, A., Tombesi, S., Gardi, T., Micheli, M., Berrios, J. G., Zadra, C., and Farinelli,
820 D. 2019. Mitigation of multiple summer stresses on hazelnut (*Corylus avellana* L.): effects
821 of the new arbuscular mycorrhiza *Glomus iranicum tenuihypharum* sp. *nova*. **Sci. Hortic.**
822 257:108659. https://doi.org/10.1016/j.scienta.2019.108659.
823 Luo, L., Zhang, J., Ye, C., Li, S., Duan, S., Wang, Z., Huang, H., Liu, Y., Deng, W., Mei, X.,
824 He, X., Yang, M., Zhu, S. 2022. Foliar pathogen infection manipulates soil health through
825 root exudate-modified rhizosphere microbiome. **Microbiol Spectr** 10:e02418-22.
826 https://doi.org/10.1128/spectrum.02418-22
827 Ma, W., Yang, Z., Liang, L., Ma, Q., Wang, G., and Zhao, T. 2021. Characteristics of the fungal
828 communities and co-occurrence networks in hazelnut tree root endospheres and rhizosphere
829 soil. **Front. Plant Sci.** 12. https://doi.org/10.3389/fpls.2021.749871.
830 Majer, H. M., Ehrlich, R. L., Ahmed, A., Earl, J. P., Ehrlich, G. D., and Beld, J. 2021. Whole
831 genome sequencing of *Streptomyces actuosus* ISP-5337, *Streptomyces sioyaensis* B-5408,
832 and *Actinospica acidiphila* B-2296 reveals secondary metabolomes with antibiotic potential.
833 **Biotechnol. Rep.** 29:e00596. https://doi.org/10.1016/j.btre.2021.e00596.
834 Martinez Arbizu, P. 2017. **pairwiseAdonis: pairwise multilevel comparison using adonis**.
835 https://github.com/pmartinezarbizu/pairwiseAdonis.
836 Matsen, F. A., Kodner, R. B., and Armbrust, E. V. 2010. pplacer: linear time maximum-likelihood
837 and Bayesian phylogenetic placement of sequences onto a fixed reference tree. **BMC**
838 **Bioinformatics** 11:538. https://doi.org/10.1186/1471-2105-11-538.

839 McMurdie, P. J., and Holmes, S. 2013. phyloseq: an R package for reproducible interactive
840 analysis and graphics of microbiome census data. **PLOS ONE** 8:e61217.
841 https://doi.org/10.1371/journal.pone.0061217.
842 Minh, B. Q., Schmidt, H. A., Chernomor, O., Schrempf, D., Woodhams, M. D., von Haeseler, A.,
843 and Lanfear, R. 2020. IQ-TREE 2: new models and efficient methods for phylogenetic
844 inference in the genomic era. **Mol. Biol. Evol.** 37:1530–1534.
845 https://doi.org/10.1093/molbev/msaa015.
846 Molnar, T. J. 2011. Corylus. Pages 15–48 in: ***Wild Crop Relatives: Genomic and Breeding***
847 ***Resources: Forest Trees***. C. Kole, ed. Springer, Heidelberg, Germany.
848 https://doi.org/10.1007/978-3-642-21250-5_2.
849 Mur, L. A. J., Simpson, C., Kumari, A., Gupta, A. K., and Gupta, K. J. 2017. Moving nitrogen to
850 the centre of plant defence against pathogens. **Ann. Bot.** 119:703–709.
851 https://doi.org/10.1093/aob/mcw179.
852 Nasir, N. N. M., Ho, C.-L., Lamasudin, D. U., and Saidi, N. B. 2020. Nitric oxide improves
853 tolerance to *Fusarium oxysporum* f. sp. cubense tropical race 4 in banana. **Physiol. Mol.**
854 **Plant Pathol.** 111:101503. https://doi.org/10.1016/j.pmpp.2020.101503.
855 Navarro-Muñoz, J. C., Selem-Mojica, N., Mullowney, M. W., Kautsar, S. A., Tryon, J. H.,
856 Parkinson, E. I., De Los Santos, E. L. C., Yeong, M., Cruz-Morales, P., Abubucker, S.,
857 Roeters, A., Lokhorst, W., Fernandez-Guerra, A., Cappelini, L. T. D., Goering, A. W.,
858 Thomson, R. J., Metcalf, W. W., Kelleher, N. L., Barona-Gomez, F., and Medema, M. H.
859 2020. A computational framework to explore large-scale biosynthetic diversity. **Nat. Chem.**
860 **Biol.** 16:60–68. https://doi.org/10.1038/s41589-019-0400-9.
861 Nissen, J. N., Johansen, J., Allesøe, R. L., Sønderby, C. K., Armenteros, J. J. A., Grønbech, C. H.,

862 Jensen, L. J., Nielsen, H. B., Petersen, T. N., Winther, O., and Rasmussen, S. 2021. Improved
863 metagenome binning and assembly using deep variational autoencoders. **Nat. Biotechnol.**
864 39:555–560. https://doi.org/10.1038/s41587-020-00777-4.
865 Oksanen, J., Simpson, G. L., Blanchet, F. G., Kindt, R., Legendre, P., Minchin, P. R., O'Hara, R.
866 B., Solymos, P., Stevens, M. H. H., Szoecs, E., Wagner, H., Barbour, M., Bedward, M.,
867 Bolker, B., Borcard, D., Carvalho, G., Chirico, M., De Caceres, M., Durand, S.,
868 Evangelista, H. B. A., FitzJohn, R., Friendly, M., Furneaux, B., Hannigan, G., Hill, M.
869 O., Lahti, L., McGlinn, D., Ouellette, M.-H., Ribeiro Cunha, E., Smith, T., Stier, A., Ter
870 Braak, C. J. F., and Weedon, J. 2024. **vegan: Community Ecology Package**.
871 https://CRAN.R-project.org/package=vegan
872 Olm, M. R., Brown, C. T., Brooks, B., and Banfield, J. F. 2017. dRep: a tool for fast and accurate
873 genomic comparisons that enables improved genome recovery from metagenomes through
874 de-replication. **ISME J.** 11:2864–2868. https://doi.org/10.1038/ismej.2017.126.
875 Ondov, B. D., Bergman, N. H., and Phillippy, A. M. 2011. Interactive metagenomic visualization
876 in a web browser. **BMC Bioinformatics** 12:385. https://doi.org/10.1186/1471-2105-12-385.
877 Ondov, B. D., Treangen, T. J., Melsted, P., Mallonee, A. B., Bergman, N. H., Koren, S., and
878 Phillippy, A. M. 2016. Mash: fast genome and metagenome distance estimation using
879 MinHash. **Genome Biol.** 17:132. https://doi.org/10.1186/s13059-016-0997-x.
880 Orozco-Mosqueda, Ma. D. C., Fadiji, A. E., Babalola, O. O., Glick, B. R., and Santoyo, G. 2022.
881 Rhizobiome engineering: unveiling complex rhizosphere interactions to enhance plant
882 growth and health. **Microbiol. Res.** 263:127137.
883 https://doi.org/10.1016/j.micres.2022.127137.
884 Pan, S., Zhao, X.-M., and Coelho, L. P. 2023. SemiBin2: self-supervised contrastive learning leads

885 to better MAGs for short- and long-read sequencing. **Bioinformatics** 39:i21–i29.
886 https://doi.org/10.1093/bioinformatics/btad209.
887 Pantigoso, H. A., Newberger, D., and Vivanco, J. M. 2022. The rhizosphere microbiome: plant–
888 microbial interactions for resource acquisition. **J. Appl. Microbiol.** 133:2864–2876.
889 https://doi.org/10.1111/jam.15686.
890 Parks, D. H., Imelfort, M., Skennerton, C. T., Hugenholtz, P., and Tyson, G. W. 2015. CheckM:
891 assessing the quality of microbial genomes recovered from isolates, single cells, and
892 metagenomes. **Genome Res.** 25:1043–1055. https://doi.org/10.1101/gr.186072.114.
893 Pedersen, T. L. 2019. **patchwork: The Composer of Plots**. http://CRAN.R-
894 project.org/package=patchwork
895 Peiffer, J. A., Spor, A., Koren, O., Jin, Z., Tringe, S. G., Dangl, J. L., Buckler, E. S., and Ley, R. E.
896 2013. Diversity and heritability of the maize rhizosphere microbiome under field conditions.
897 **Proc. Natl. Acad. Sci.** 110:6548–6553. https://doi.org/10.1073/pnas.1302837110.
898 Pinkerton, J. N. 1995. Infection of European hazelnut by *Anisogramma anomala*: ascospore
899 adhesion, mode of penetration of immature shoots, and host response. **Phytopathology**
900 85:1260. https://doi.org/10.1094/Phyto-85-1260.
901 Poomthongdee, N., Duangmal, K., and Pathom-aree, W. 2015. Acidophilic actinomycetes from
902 rhizosphere soil: diversity and properties beneficial to plants. **J. Antibiot.** 68:106–114.
903 https://doi.org/10.1038/ja.2014.117.
904 Puopolo, G., Giovannini, O., and Pertot, I. 2014. *Lysobacter capsici* AZ78 can be combined with
905 copper to effectively control *Plasmopara viticola* on grapevine. **Microbiol. Res.** 169:633–
906 642. https://doi.org/10.1016/j.micres.2013.09.013.
907 Qi, G., Ma, G., Chen, S., Lin, C., and Zhao, X. 2019. Microbial network and soil properties are

908 changed in bacterial wilt-susceptible soil. **Appl. Environ. Microbiol.** 85:e00162-19.
909 https://doi.org/10.1128/AEM.00162-19.
910 Qiao, H., Gao, D., and Yuan, T. 2023. Differences in rhizosphere soil fungal communities of wild
911 and cultivated *Paeonia ludlowii* species. **Front. Plant Sci.** 14.
912 https://doi.org/10.3389/fpls.2023.1194598.
913 Ranjan, A., Rajput, V. D., Prazdnova, E. V., Gurnani, M., Bhardwaj, P., Sharma, S., Sushkova, S.,
914 Mandzhieva, S. S., Minkina, T., Sudan, J., Zargar, S. M., Chauhan, A., and Jindal, T. 2023.
915 Nature's antimicrobial arsenal: non-ribosomal peptides from PGPB for plant pathogen
916 biocontrol. **Fermentation** 9:597. https://doi.org/10.3390/fermentation9070597.
917 R Core Team. 2025. The R Project for Statistical Computing. https://www.R-project.org/
918 Revord, R. S., Lovell, S. T., Capik, J. M., Mehlenbacher, S. A., and Molnar, T. J. 2020. Eastern
919 filbert blight resistance in American and interspecific hybrid hazelnuts. **J. Am. Soc. Hortic.**
920 **Sci.** 145:162–173. https://doi.org/10.21273/JASHS04732-19.
921 Rodriguez-Mena, S., Camacho, M., de los Santos, B., Miranda, L., and Camacho-Sanchez, M.
922 2022. Microbiota modulation in blueberry rhizosphere by biocontrol bacteria. **Microbiol.**
923 **Res.** 13:809–824. https://doi.org/10.3390/microbiolres13040057.
924 Rostamikia, Y., Tabari Kouchaksaraei, M., Asgharzadeh, A., and Rahmani, A. 2017. Effect of
925 growth promoting rhizobacteria on growth and nutrient elements of common hazelnut
926 (*Corylus avellana* L.) seedlings in Ardabil Fandoqlou nursery. **Iran. J. For. Poplar Res.**
927 25:126–116. https://doi.org/10.22092/ijfpr.2017.109781.
928 Ruparelia, J., Rabari, A., Mitra, D., Panneerselvam, P., Das-mohapatra, P. K., and Jha, C. K. 2022.
929 Efficient applications of bacterial secondary metabolites for management of biotic stress in
930 plants. **Plant Stress** 6:100125. https://doi.org/10.1016/j.stress.2022.100125.

931 Santoyo, G. 2022. How plants recruit their microbiome? New insights into beneficial interactions.
932 **J. Adv. Res.** 40:45–58. https://doi.org/10.1016/j.jare.2021.11.020.
933 Shaffer, M., Borton, M. A., McGivern, B. B., Zayed, A. A., La Rosa, S. L., Solden, L. M., Liu, P.,
934 Narrowe, A. B., Rodríguez-Ramos, J., Bolduc, B., Gazitúa, M. C., Daly, R. A., Smith, G. J.,
935 Vik, D. R., Pope, P. B., Sullivan, M. B., Roux, S., and Wrighton, K. C. 2020. DRAM for
936 distilling microbial metabolism to automate the curation of microbiome function. **Nucleic**
937 **Acids Res.** 48:8883–8900. https://doi.org/10.1093/nar/gkaa621.
938 Sharrar, A. M., Crits-Christoph, A., Méheust, R., Diamond, S., Starr, E. P., and Banfield, J. F. 2020.
939 Bacterial secondary metabolite biosynthetic potential in soil varies with phylum, depth, and
940 vegetation type. **mBio** 11:e00416-20. https://doi.org/10.1128/mBio.00416-20.
941 Sieber, C. M. K., Probst, A. J., Sharrar, A., Thomas, B. C., Hess, M., Tringe, S. G., and Banfield,
942 J. F. 2018. Recovery of genomes from metagenomes via a dereplication, aggregation and
943 scoring strategy. **Nat. Microbiol.** 3:836–843. https://doi.org/10.1038/s41564-018-0171-1.
944 Sillo, F., Brunetti, C., Marroni, F., Vita, F., dos Santos Nascimento, L. B., Vizzini, A., Mello, A.,
945 and Balestrini, R. 2022. Systemic effects of *Tuber melanosporum* inoculation in two *Corylus*
946 *avellana* genotypes. **Tree Physiol.** 42:1463–1480. https://doi.org/10.1093/treephys/tpac012.
947 Sood, M., Kapoor, D., Kumar, V., Sheteiwy, M. S., Ramakrishnan, M., Landi, M., Araniti, F., and
948 Sharma, A. 2020. Trichoderma: The "secrets" of a multitalented biocontrol agent. **Plants**
949 9:762. https://doi.org/10.3390/plants9060762.
950 Steinegger, M., and Söding, J. 2017. MMseqs2 enables sensitive protein sequence searching for
951 the analysis of massive data sets. **Nat. Biotechnol.** 35:1026–1028.
952 https://doi.org/10.1038/nbt.3988.
953 Sun, C., Zhang, Y., Liu, L., Liu, X., Li, B., Jin, C., and Lin, X. 2021. Molecular functions of nitric

954 oxide and its potential applications in horticultural crops. **Hortic. Res.** 8:1–17.
955 https://doi.org/10.1038/s41438-021-00500-7.
956 Sun, Y., Wang, M., Mur, L. A. J., Shen, Q., and Guo, S. 2020. Unravelling the roles of nitrogen
957 nutrition in plant disease defenses. **Int. J. Mol. Sci.** 21:572.
958 https://doi.org/10.3390/ijms21020572.
959 Thepbandit, W., and Athinuwat, D. 2024. Rhizosphere microorganisms supply availability of soil
960 nutrients and induce plant defense. **Microorganisms** 12:558.
961 https://doi.org/10.3390/microorganisms12030558.
962 Thompson, M. M., Lagerstedt, H. B., and Mehlenbacher, S. A. 1996. Hazelnuts. Pages 125–184
963 in: **Fruit Breeding, vol. III Nuts.** J. Janick, and N. Moore, eds. John Wiley and Sons Inc,
964 New York, U.S.A.
965 Wang, Y., Yang, Q., Tosa, Y., Nakayashiki, H., and Mayama, S. 2005. Nitric oxide-overproducing
966 transformants of *Pseudomonas fluorescens* with enhanced biocontrol of tomato bacterial
967 wilt. J. **Gen. Plant Pathol.** 71:33–38. https://doi.org/10.1007/s10327-004-0157-0.
968 Wattenburger, C. J., Halverson, L. J., and Hofmockel, K. S. 2019. Agricultural management affects
969 root-associated microbiome recruitment over maize development. **Phytobiomes J.** 3:260–
970 272. https://doi.org/10.1094/PBIOMES-03-19-0016-R.
971 Wickham, H. 2009. **ggplot2: Elegant Graphics for Data Analysis**. Springer, New York, U.S.A.
972 https://doi.org/10.1007/978-0-387-98141-3
973 Wickham, H., François, R., Henry, L., and Müller, K. 2018. **dplyr: A Grammar of Data**
974 **Manipulation**. https://CRAN.Rproject.org/package=dplyr.
975 Wickham, H., Averick, M., Bryan, J., Chang, W., McGowan L. D., François, R., Grolemund, G.,
976 Hayes, A., Henry, L., Hester, J., Kuhn, M., Pedersen, T. L., Miller, E., Bache S. M.,

977 Müller, K., Ooms, J., Robinson, D., Seidel, D. P., Spinu, V., Takahashi, K., Vaughan, D.,
978 Wilke, C., Woo, K., Yutani, H. 2019. Welcome to the tidyverse. **Journal of Open Source**
979 **Software** 4:1686. https://doi.org/10.21105/joss.01686>
980 Wood, D. E., Lu, J., and Langmead, B. 2019. Improved metagenomic analysis with Kraken
981 **Genome Biol.** 20:257. https://doi.org/10.1186/s13059-019-1891-0.
982 Wu, Y.-W., Simmons, B. A., and Singer, S. W. 2016. MaxBin 2.0: an automated binning algorithm
983 to recover genomes from multiple metagenomic datasets. **Bioinformatics** 32:605–607.
984 https://doi.org/10.1093/bioinformatics/btv638.
985 Yang, J., Wei, S., Su, D., Zhang, Z., Chen, S., Luo, Z., Shen, X., Lai, Y., Jamil, A., Tong, J., and
986 Cui, X. 2020. Comparison of the rhizosphere soil microbial community structure and
987 diversity between powdery mildew-infected and noninfected strawberry plants in a
988 greenhouse by high-throughput sequencing technology. **Curr. Microbiol.** 77:1724–1736.
989 https://doi.org/10.1007/s00284-020-01948-x.
990 Yu, Y., Gui, Y., Li, Z., Jiang, C., Guo, J., and Niu, D. 2022. Induced systemic resistance for
991 improving plant immunity by beneficial microbes. **Plants** 11:386.
992 https://doi.org/10.3390/plants11030386.
993 Yue, H., Yue, W., Jiao, S., Kim, H., Lee, Y.-H., Wei, G., Song, W., and Shu, D. 2023. Plant
994 domestication shapes rhizosphere microbiome assembly and metabolic functions.
995 **Microbiome** 11:70. https://doi.org/10.1186/s40168-023-01513-1.
996 Zhang, F., Wen, S., Wang, B., Zhang, Z., Liu, F., Ye, T., Wang, K., Hu, H., Yang, X., and Fang, W.
997 2023. Biocontrol potential of *Streptomyces odonnellii* SZF-179 toward *Alternaria alternata*
998 to control pear black spot disease. **Int. J. Mol. Sci.** 24:17515.
999 https://doi.org/10.3390/ijms242417515.

1000 Zhang, J., Cook, J., Nearing, J. T., Zhang, J., Raudonis, R., Glick, B. R., Langille, M. G. I., and
1001 Cheng, Z. 2021. Harnessing the plant microbiome to promote the growth of agricultural
1002 crops. **Microbiol. Res.** 245:126690. https://doi.org/10.1016/j.micres.2020.126690.
1003 Zhang, M., Chai, L., Huang, M., Jia, W., Guo, J., and Huang, Y. 2020. Deciphering the archaeal
1004 communities in tree rhizosphere of the Qinghai-Tibetan plateau. **BMC Microbiol.** 20:235.
1005 https://doi.org/10.1186/s12866-020-01913-5.
1006

1007 **FIGURE LEGENDS**

1008 **Figure 1. Diversity metrics of the metagenomes.** (**A**, **B**) Alpha diversity values calculated using
1009 the (A) Shannon Diversity Index (Kruskal-Wallis rank sum test, p-value = 0.16) or (B) Simpson
1010 Diversity Index [1-D] (Kruskal-Wallis rank sum test, p-value = 0.06) are shown. Alpha diversity
1011 was calculated based on species level taxonomic classification of assembled contigs (minimum
1012 length of 500 bp). (**C**) A Principal Coordinate Analysis (PCoA) plot based on Bray-Curtis
1013 dissimilarity values is shown (PERMANOVA, p-value < 0.001), with pairwise adonis tests
1014 indicating that the bulk soil was statistically different from the rhizospheres of the native
1015 (p.adjusted = 0.048), susceptible (p.adjusted = 0.047), and resistant (p.adjusted = 0.047) varieties.
1016

1017 **Figure 2. Relative abundance of phyla across the metagenomes.** The abundance of (**A**) bacterial
1018 phyla, (**B**) archaeal phyla, and (**C**) eukaryotic phyla, displayed as a percentage of the total bacteria,
1019 archaea, and eukaryotes, respectively. The rows represent each of the metagenomic samples,
1020 colour coded by group, while the columns represent taxa with an average relative abundance of at
1021 least 1% of the bacteria, archaea, or eukaryotes, respectively. The size of the dots corresponds is
1022 proportional to the relative abundance of the taxon in a given sample, as indicated by the legend
1023 to the right of the figure.
1024

1025 **Figure 3. Relative abundance of genera across the metagenomes.** The abundance of (**A**)
1026 bacterial genera, (**B**) archaeal genera, and (**C**) eukaryotic genera, displayed as a percentage of the
1027 total bacteria, archaea, and eukaryotes, respectively. The rows represent each of the metagenomic
1028 samples, colour coded by group, while the columns represent taxa with an average relative
1029 abundance of at least 1% of the bacteria, archaea, or eukaryotes, respectively. The size of the dots

1030 corresponds is proportional to the relative abundance of the taxon in a given sample, as indicated
1031 by the legend to the right of the figure. (**D**) A heatmap showing the differential abundances of
1032 bacterial genera identified as showing statistically significant differences in abundances across
1033 treatments. Columns were scaled using pheatmap in R. Dark red indicates higher abundances while
1034 dark blue indicates lower abundances.
1035
1036 **Figure 4. Global comparison of the metabolic potential of the metagenomes.** A Principal
1037 Coordinate Analysis (PCoA) plot based on Bray-Curtis dissimilarity values calculated from the
1038 KEGG annotations produced for each metagenome using DRAM. While statistically significant
1039 global differences were observed (PERMANOVA, p-value = 0.031), no statistically significant
1040 differences between groups were detected using pairwise adonis tests.
1041
1042 **Figure 5. Putative biosynthetic gene clusters detected in the metagenomes.** (**A**) A heatmap
1043 showing distribution of predicted biosynthetic gene clusters summarized by biosynthetic gene
1044 cluster classification. (**B**) A heatmap showing the distribution of predicted biosynthetic gene
1045 clusters summarized by predicted product. (**A**, **B**) A coloured box indicates that a biosynthetic
1046 gene cluster classification or predicted product was detected in a given metagenome, whereas a
1047 white box indicates that the pathway was not detected.
1048
1049 **Figure 6. Unrooted phylogeny of the bacterial MAGs generated in this study.** An unrooted,
1050 maximum likelihood phylogeny of the 41 high-quality metagenome-assembled genomes (MAGs)
1051 generated in this study, prepared from a concatenated alignment of the bac120 gene set of the
1052 Genome Taxonomy Database. Taxa names and branches are colour coded based on phylum. The

1053 scale represents the mean number of nucleotide substitutions per site. The numbers on the nodes
1054 indicate the SH-aLRT support values (top numbers) and the ultra-fast jackknife values using a
1055 40% resampling rate (bottom numbers), both calculated from 1000 replicates; values are only
1056 shown at nodes where at least one value is below 95.
1057

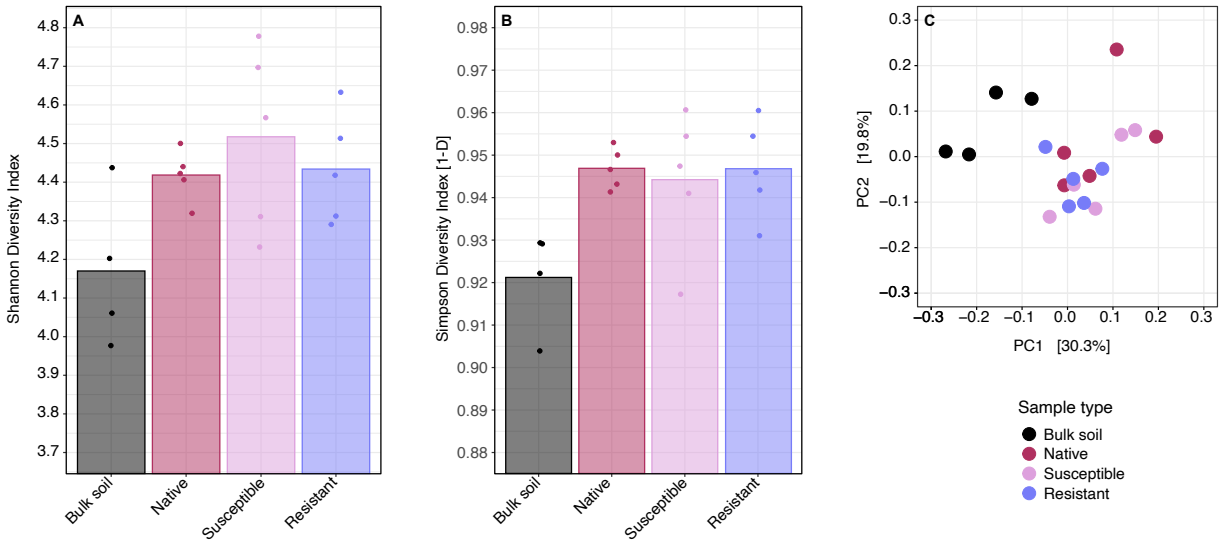

Figure 1. Diversity metrics of the metagenomes. (**A**, **B**) Alpha diversity values calculated using the (A) Shannon Diversity Index (Kruskal-Wallis rank sum test, p-value = 0.16) or (B) Simpson Diversity Index [1-D] (Kruskal-Wallis rank sum test, p-value = 0.06) are shown. Alpha diversity was calculated based on species level taxonomic classification of assembled contigs (minimum length of 500 bp). (**C**) A Principal Coordinate Analysis (PCoA) plot based on Bray-Curtis dissimilarity values is shown (PERMANOVA, p-value < 0.001), with pairwise adonis tests indicating that the bulk soil was statistically different from the rhizospheres of the native (p.adjusted = 0.048), susceptible (p.adjusted = 0.047), and resistant (p.adjusted = 0.047) varieties.

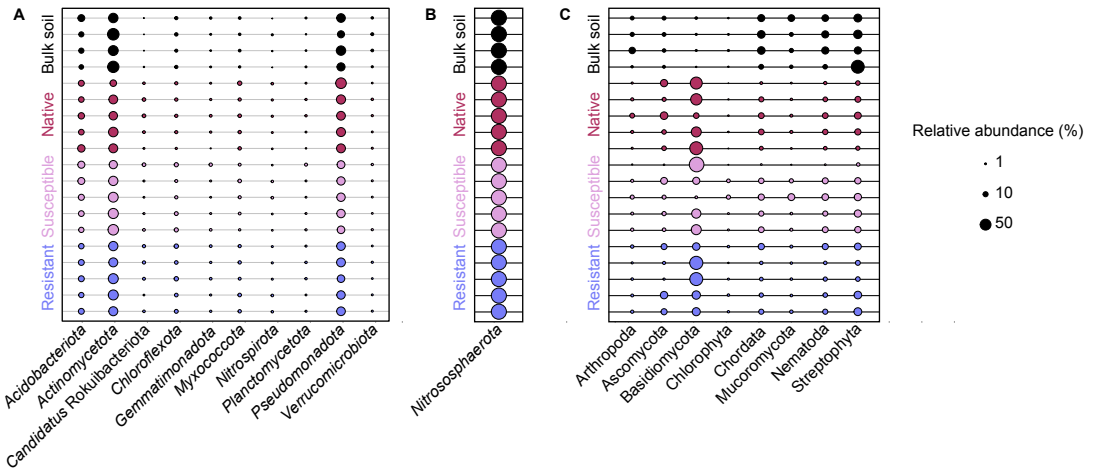

Figure 2. Relative abundance of phyla across the metagenomes. The abundance of (**A**) bacterial phyla, (**B**) archaeal phyla, and (**C**) eukaryotic phyla, displayed as a percentage of the total bacteria, archaea, and eukaryotes, respectively. The rows represent each of the metagenomic samples, colour coded by group, while the columns represent taxa with an average relative abundance of at least 1% of the bacteria, archaea, or eukaryotes, respectively. The size of the dots corresponds is proportional to the relative abundance of the taxon in a given sample, as indicated by the legend to the right of the figure.

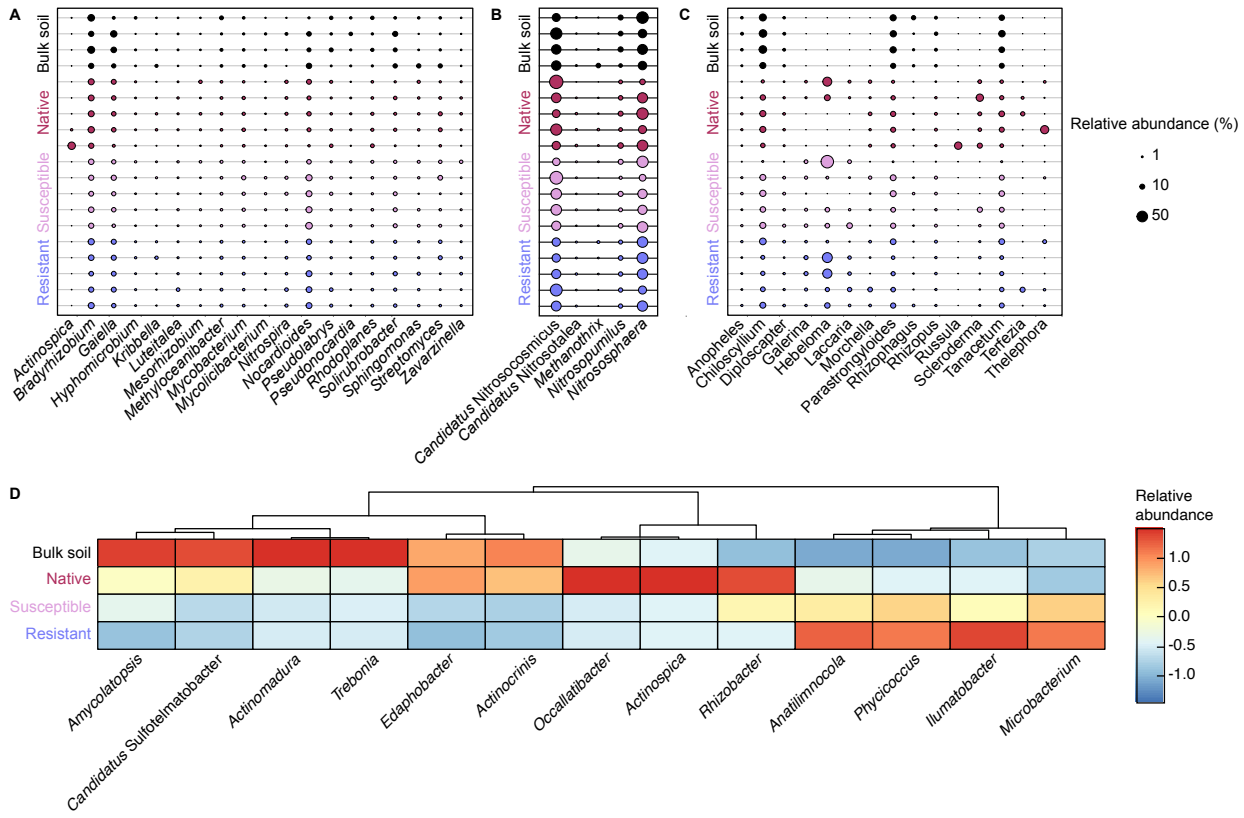

Figure 3. Relative abundance of genera across the metagenomes. The abundance of (**A**) bacterial genera, (**B**) archaeal genera, and (**C**) eukaryotic genera, displayed as a percentage of the total bacteria, archaea, and eukaryotes, respectively. The rows represent each of the metagenomic samples, colour coded by group, while the columns represent taxa with an average relative abundance of at least 1% of the bacteria, archaea, or eukaryotes, respectively. The size of the dots corresponds is proportional to the relative abundance of the taxon in a given sample, as indicated by the legend to the right of the figure. (**D**) A heatmap showing the differential abundances of bacterial genera identified as showing statistically significant differences in abundances across treatments. Columns were scaled using pheatmap in R. Dark red indicates higher abundances while dark blue indicates lower abundances.

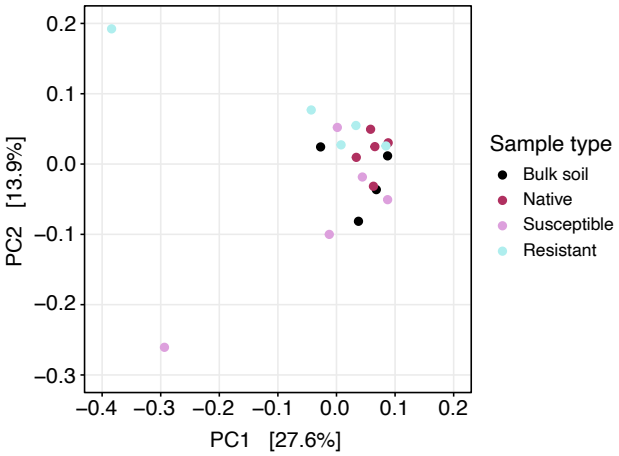

1089
1090
1091 **Figure 4. Global comparison of the metabolic potential of the metagenomes.** A Principal
1092 Coordinate Analysis (PCoA) plot based on Bray-Curtis dissimilarity values calculated from the
1093 KEGG annotations produced for each metagenome using DRAM. While statistically significant
1094 global differences were observed (PERMANOVA, p-value = 0.031), no statistically significant
1095 differences between groups were detected using pairwise adonis tests.

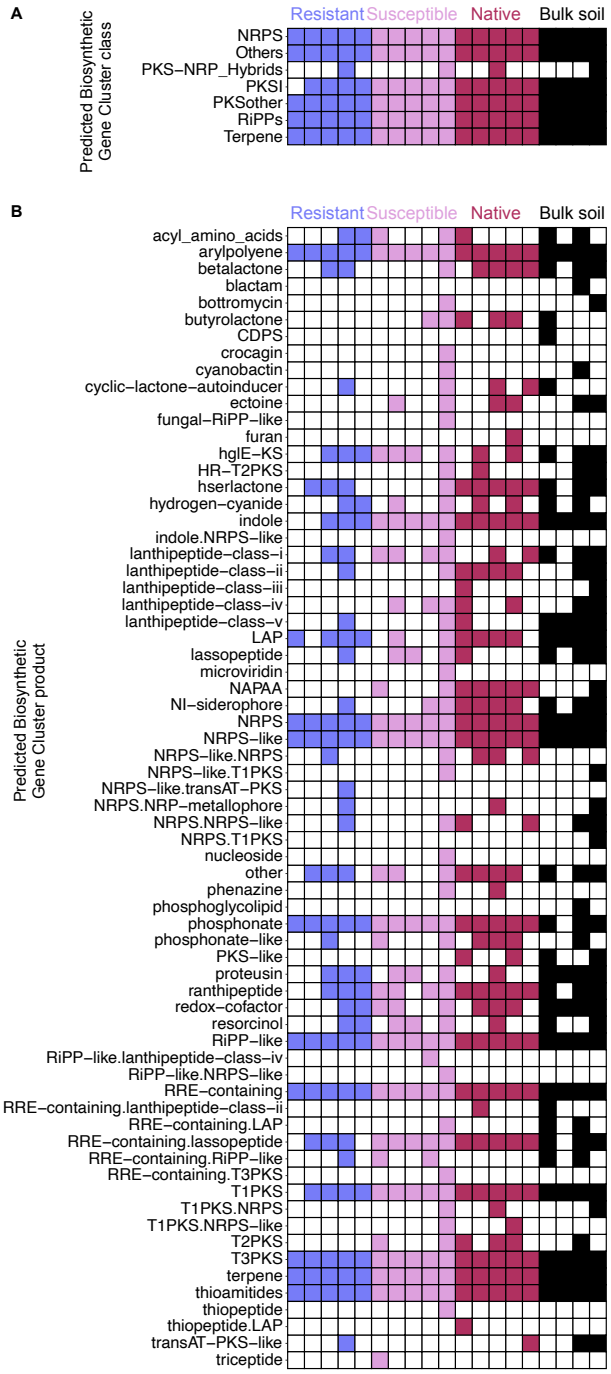

Figure 5. Putative biosynthetic gene clusters detected in the metagenomes. (**A**) A heatmap showing distribution of predicted biosynthetic gene clusters summarized by biosynthetic gene cluster classification. (**B**) A heatmap showing the distribution of predicted biosynthetic gene clusters summarized by predicted product. (**A**, **B**) A coloured box indicates that a biosynthetic gene cluster classification or predicted product was detected in a given metagenome, whereas a white box indicates that the pathway was not detected.

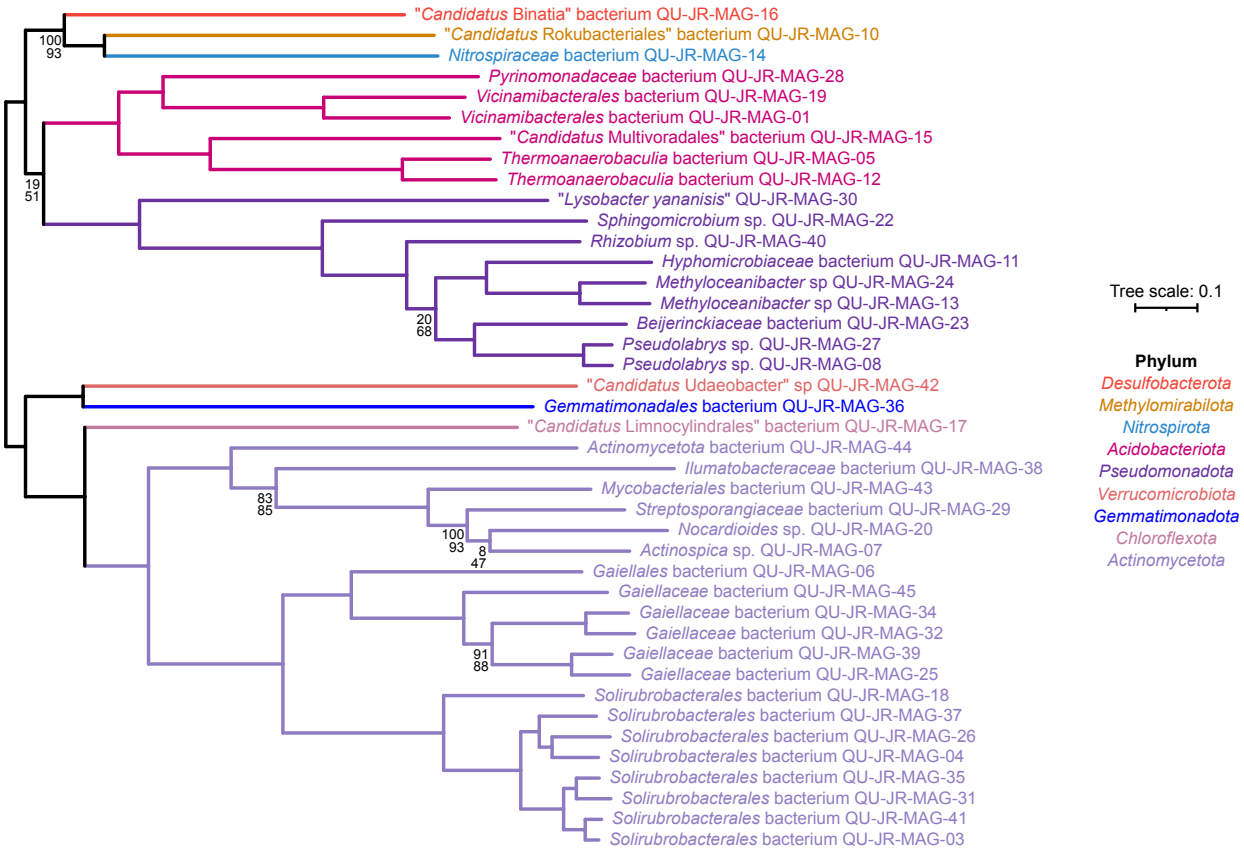

Figure 6. Unrooted phylogeny of the bacterial MAGs generated in this study. An unrooted, maximum likelihood phylogeny of the 41 high-quality metagenome-assembled genomes (MAGs) generated in this study, prepared from a concatenated alignment of the bac120 gene set of the Genome Taxonomy Database. Taxa names and branches are colour coded based on phylum. The scale represents the mean number of nucleotide substitutions per site. The numbers on the nodes indicate the SH-aLRT support values (top numbers) and the ultra-fast jackknife values using a 40% resampling rate (bottom numbers), both calculated from 1000 replicates; values are only shown at nodes where at least one value is below 95.